CPM-SC-IFDMA—A Power Efficient Transmission Scheme for Uplink LTE

Raina Rahman

Submitted to the graduate degree program in Electrical Engineering and Computer Science and the Graduate Faculty of the University of Kansas in partial fulfillment of the requirements for the degree of Master of Science.

Thesis Committee:

Dr. Erik Perrins: Chairperson

Dr. K Sam Shanmugan

Dr. Shannon Blunt

Date Defended

The Thesis Committee for Raina Rahman certifies
that this is the approved version of the following thesis:

**CPM-SC-IFDMA—A Power Efficient Transmission Scheme for
Uplink LTE**

Committee:

_____

Chairperson: Dr. Erik Perrins

_____

_____

_____

Date Approved

To my mother

Acknowledgments

I am grateful to Allah, for giving me the strength and courage to complete my graduate studies at KU, despite all the difficulties that I have been through.

I owe my deepest gratitude to my adviser, Dr. Erik Perrins, for giving me the opportunity to work on this project, for all his valuable advice and guidance, and most of all, for giving me the encouragement and mental support at a very difficult time of my life. It would not have been possible for me to continue my studies without his support. I want to thank Dr. Marilynn Green for her advice on the thesis, which helped me develop a better understanding of the topic. I am also thankful to Dr. Shanmugan and Dr. Blunt for taking time to serve on my committee and reviewing this thesis.

I thank my mother for her love and support. I also want to thank Mahmud, my husband, my best friend for the last six years, for all the sacrifices that he has made for me, and for making me smile even at my most troubled times.

Lastly, I thank all my professors, friends and colleagues at KU, for their help and support.

Abstract

In this thesis we have proposed a power efficient transmission scheme, CPM-SC-IFDMA, for uplink LTE. In uplink LTE, efficiency of the transmitter power amplifier is a major concern, as the transmitter is placed in the mobile device which has limited power supply. The proposed scheme, CPM-SC-IFDMA, combines the key advantages of CPM (continuous phase modulation) with SC-IFDMA (single carrier frequency division multiple access with interleaved subcarrier mapping) in order to increase the power amplifier efficiency of the transmitter.

In this work, we have analyzed the bit error rate (BER) performance of the proposed scheme in LTE specified channels. The BER performance of two CPM-SC-IFDMA scheme are compared with that of a LTE specified transmission scheme, QPSK-LFDMA (QPSK modulated SC-FDMA with localized subcarrier mapping), combined with convolutional coding (CC-QPSK-LFDMA). We first show that CPM-SC-IFDMA has a much higher power efficiency than CC-QPSK-LFDMA by simulating the PAPR (peak-to-average-power-ratio) plots. Then, using the data from the PAPR plots and the conventional BER plots (BER as a function of signal-to-noise-ratio), we show that, when the net BER, obtained by compensating for the power efficiency loss, is considered, CPM-SC-IFDMA has a superior performance relative to CC-QPSK-LFDMA by up to 3.8 dB, in the LTE specified channels.

Contents

List of Figures

viii

List of Tables

Chapter 1

Introduction

1.1 Background

LTE (Long Term Evolution) is a new high performance air interface for cellular mobile communication systems developed by the 3rd Generation Partnership Project (3GPP), a collaboration between groups of telecommunications associations. LTE represents a major advance in cellular technology. It is the next step in a continuous move to wider bandwidths and higher data rates. LTE is expected to be the next major standard in mobile broadband technology that promises to enhance the delivery of mobile broadband services through a combination of very high transmission speeds, more flexible and efficient use of spectrum, and reduced packet latency.

To fulfill its ambitious requirements for spectral efficiency and high data rate, LTE has selected Orthogonal Frequency Division Multiple Access (OFDMA) as the multiple access scheme for uplink. OFDMA is an extension of OFDM (Orthogonal Frequency Division Multiplexing) to accommodate multiple users. OFDM, being a multi-carrier modulation method, offers a number of advantages including

high data rate, robustness against interference in multipath fading channels, and simple implementation methods. But the major disadvantage with OFDM is the high Peak-to-Average-Power-Ratio (PAPR) caused by the superposition of all subcarrier signals. High PAPR tends to cause non-linear distortion in the RF power amplifier that transmits the radio frequency signal via the antenna. To avoid distortion, the power amplifier needs input power reduction (*input power back-off*), which leads to poor power efficiency and shorter battery life [1, Chapter 4].

Battery life represents a key concern in the mobile communication field. As device miniaturization is progressing at a faster rate than battery technology optimization, battery life often places a limitation on the utility of the mobile devices. The RF power amplifier has the highest power consumption within the mobile device. Therefore, in order to ensure that mobile devices use as little battery power as possible, efficient operation of the RF amplifiers is required. However, this problem is not as much of a concern in the downlink as in the uplink.

In the downlink, where the signal is transmitted from the base station to the mobile device, the transmitter is placed in the base station, where power supply is not a problem. Whereas in the uplink, the signal is transmitted from the mobile device to the base station, and the transmitter is placed in the mobile device, which has limited power resources. Hence, for uplink LTE, 3GPP has chosen SC-FDMA (Single Carrier Frequency Division Multiple Access), which is similar to OFDMA, but instead of transmitting the subcarriers in parallel, SC-FDMA spreads the symbols throughout all the subcarriers and transmits them sequentially. As a result, the PAPR is very low in an SC-FDMA system.

1.2 Motivation to Develop a New Transmission Scheme for Uplink LTE

The modulation method and multiple access scheme that LTE uses have some drawbacks. The modulation schemes currently specified in LTE are QPSK, 16QAM and 64QAM. But the phase discontinuity in these methods gives rise to out-of-band radiation, which leads to poor power efficiency and higher bandwidth requirement [2]. For multiple access, LTE specifies SC-FDMA with localized subcarrier mapping (LFDMA) (Section 3.4), where the data from each user is mapped to a set of adjacent subcarriers. LFDMA, despite being a single carrier multiple access scheme with lower PAPR than OFDMA, has more envelope fluctuations and higher peak power in the time-domain transmitted signal, compared to other subcarrier mapping methods. Myung and Goodman in [3] showed that in LFDMA, the transmitted time domain signal is an interpolation of the original input symbols, which contains both weighted sums and the actual input symbols. As a result, the transmitted signal does not have a constant envelope, and the PAPR becomes high.

1.3 Proposed Transmission Scheme

In this work we propose CPM-SC-IFDMA, a novel multiple access transmission scheme which combines the key features of CPM and SC-IFDMA and is highly power efficient. In the proposed scheme, the CPM (Continuous Phase Modulation) modulated continuous-time waveform from each user is first sampled, and then the discrete time samples are transmitted using the SC-FDMA multiple access method with an interleaved subcarrier mapping (IFDMA) (Section 3.4). In the receiver,

after the effect of the multipath channel is removed, the Viterbi Algorithm (VA) is applied for detecting the symbols.

We have selected CPM as the modulation method because of its high power and spectral efficiency. CPM has high spectral efficiency due to its continuous phase nature. The PAPR is always unity for a CPM waveform since it has a constant envelope, which yields excellent power efficiency. For multiple access, we have chosen SC-FDMA with interleaved subcarrier mapping (IFDMA), instead of LFDMA. Again, the motivation for making this choice comes from the ability of IFDMA to maintain a very low PAPR. In IFDMA the transmitted time domain signal contains a scaled and phase rotated version of the actual input symbols, as Myung and Goodman showed in [3]. Therefore, the transmitted signal amplitude in IFDMA is determined by the input symbols; if the input symbols have a constant amplitude, so will the transmitted signal.

Our goal is to select a modulation method with the lowest PAPR and combine it with a single carrier based multiple access scheme that retains the low PAPR property of this method. In the proposed transmission scheme, the discrete-time, constant amplitude samples from the CPM waveform can be treated as the input "symbols" to the SC-IFDMA system, which can be DFT-precoded and mapped to a set of orthogonal subcarriers with an interleaved subcarrier mapping for multiple access. The resultant time-domain signal that is transmitted maintains the constant envelope properties of CPM. This is not possible with LFDMA due to its inherent property of envelope fluctuations. With unity PAPR the required input power back-off is 0 dB; i.e., no input power back-off is necessary. Therefore the RF power amplifier can operate in the most efficient point (saturation), which maximizes battery life. Thus, by combining the key features of CPM and SC-

IFDMA, we can develop a power efficient scheme, which is ideal for applications where battery life and device miniaturization are identified as the key concerns and makes an excellent choice for uplink LTE.

1.4 Previous Work

Our work is based on the results and observations presented in [4]. Green et al. in [4], showed the PAPR, spectral performance, and error performance of two CPM-SC-IFDMA schemes (Scheme 1 and Scheme 2) and compared with those of a convolutionally coded QPSK modulated SC-IFDMA (CC-QPSK-IFDMA) scheme. Both schemes were shown to have much lower PAPR than CC-QPSK-IFDMA. The Power Spectral Density (PSD) plots showed that Scheme 1 has the narrowest spectrum, while Scheme 2 with roll-off close to 0 has a very similar bandwidth to CC-QPSK-IFDMA, assuming that the channel bandwidth is defined at a sidelobe decay level around -20 dB. The bit error rate performances of Scheme 1, Scheme 2, and CC-QPSK-IFDMA were demonstrated in [4] for the AWGN channel and two frequency-selective channels: the ITU Pedestrian A (PedA) channel and the ITU Vehicular A (VehA) channel [5]. According to the results found in [4], when the input power back-off values are taken into account, the BER performance of CC-QPSK-IFDMA gets much worse than that of the CPM-SC-IFDMA schemes.

1.5 Contribution of This Thesis

Our work has a similar structure as [4], however, we have done the simulations according to the specifications of 3GPP LTE, and instead of a CC-QPSK-IFDMA

scheme, we chose a CC-QPSK-LFDMA (convolutionally coded QPSK modulated SC-FDMA scheme with a localized subcarrier mapping) scheme for performance comparison, since LFDMA is the subcarrier mapping method that LTE specifies. We have shown the bit error rate (BER) performances of two CPM-SC-IFDMA schemes and the CC-QPSK-LFDMA scheme in the AWGN channel and three frequency selective fading channels: the Extended Pedestrian A (EPA) channel, the Extended Vehicular A (EVA) channel, and the Extended Typical Urban (ETU) channel. The channel delay profiles were taken from the 3GPP specification of LTE [6]. Also, we applied Maximal Ratio Combining (MRC) at the receiver with a two-antenna structure, in accordance with the LTE specifications, to enhance link reliability in challenging propagation conditions.

1.6 Organization

The thesis is organized as follows. In Chapter 2, we present a brief description of LTE, where we discuss the basic features of LTE. In Chapter 3, we discuss the different properties of SC-FDMA. We show the similarities and dissimilarities of SC-FDMA with OFDMA technology. We also discuss the benefits of the interleaved subcarrier mapping over the localized one. Chapter 4 presents a review of the CPM basics, including a brief analysis on effect of the basic CPM parameters on the performance of a CPM scheme. Chapter 4 also explains the CPM-SC-IFDMA signal model. Chapter 5 focuses on applying the proposed CPM-SC-IFDMA scheme in LTE. We discuss the advantage of the proposed scheme over the current transmission scheme specified in LTE. Finally, we summarize the simulation results in Chapter 6, followed by a brief conclusion in Chapter 7.

Chapter 2

LTE Overview

3GPP initiated the project of defining the Long Term Evolution (LTE) in 2004 to ensure its competitive edge over other cellular technologies. Building on the technical foundations of the 3GPP family of cellular systems that embraces GSM (Global System for Mobile Communication), GPRS (General Packet Radio Service) and EDGE (Enhanced Data Rates for GSM Evolution) as well as WCDMA (Wide Band Code Division Multiple Access) and now HSPA (High Speed Packet Access), LTE offers a smooth evolutionary path to better data speeds and spectral efficiency. The first version of LTE is documented in Release 8 of the 3GPP specifications. In the earlier 3GPP releases, the specifications related to this effort were known as E-UTRA (Evolved UMTS Terrestrial Radio Access) and E-UTRAN (Evolved UMTS Terrestrial Radio Access Network), but now these are more commonly referred to by the project name LTE. In addition to LTE, 3GPP is also defining an IP-based, flat, packet-only network architecture known as EPC (Evolved Packet Core). This new architecture is defined as part of the System Architecture Evolution (SAE) effort and has been developed to provide a considerably higher level of performance that is in line with the requirements of

LTE. In this Chapter, first we briefly mention the 3rd generation technologies that preceeded LTE, and then we present an overview of LTE including performance requirement, physical layer, and frame structure. Additional information on the topics covered in this section can be found in [7–9].

2.1 Evolution of 3GPP Specification Towards LTE

Each release of the 3GPP specifications represents a defined set of features of a technological standard. In Release 99, 3GPP specified UMTS (Universal Mobile Telecommunication System), the third generation technology which is based on WCDMA (Wide Band Code Division Multiple Access). UMTS was the next step after GSM, GPRS, and EDGE, to offer improved voice and data services with a 5 MHz bandwidth. Following this was Release 4 that introduced the 1.28 Mcps narrow band version of W-CDMA, also known as Time Domain Synchronous Code Division Multiple Access (TD-SCDMA). The rapid growth of UMTS led to the next step in the evolutionary phase: introduction of packed based data services. High speed downlink packet access (HSDPA) and High speed uplink packet access (HSUPA), specified in Release 5 and 6 respectively and known collectively as high speed packet access (HSPA), introduced packet-based data services to UMTS in the same way that GPRS did for GSM in Release 97 (1998). Evolved HSPA, also referred to as HSPA+, was defined in 3GPP Release 7 and 8, with the objective to further enhance the HSPA based radio networks and is considered to be the "missing link" between HSPA and LTE. The main work in Release 8, however, is the specification of LTE and SAE.

The current UMTS-HSPA systems have the capacity of supporting high speed packet access for both downlink (up to 14 Mbps) and uplink (up to 5.76 Mbps).

Even though HSPA services offered significant improvement for packet data transmission over earlier UMTS systems, their designs are limited by compatibility requirements with previous generations of UMTS specifications. Wireless data usage is expected to continue increasing significantly over the next years, which would require faster networks and radio interfaces, and also better cost efficiency than what is possible by the evolution of the current standards. 3GPP-LTE, on the other hand, will provide an all-new radio platform that adopts new techniques such as OFDMA/SC-FDMA and MIMO for its wireless system and is based on a new network architecture. The aim of the 3GPP-LTE project is to improve the current UMTS-HSPA systems and provide an enhanced user experience and simplified technology for next generation mobile broadband. LTE also aims for a smooth evolution from earlier 3GPP systems such as TD-SCDMA and UMTS-HSPA to give the service providers the ability to deliver a seamless mobility experience.

2.2 Performance Requirements for LTE

LTE is expected to efficiently support mobile Internet as well as a variety of wireless applications such as HTTP, FTP, real-time and non-real-time video streaming, VoIP, interactive gaming. Therefore, LTE has been designed to provide very high data rate and low air-link access latency in order to satisfy the requirements for the existing and emerging applications.

The main requirements for the design of an LTE system, can be summarized as follows [10]:

- Increased data rates: Peak data rate up to 100 Mbps for downlink and 50 Mbps for uplink within a 20 MHz spectrum allocation, assuming two receive

antennas and one transmit antenna;

- Higher spectral efficiency: $2 - 4$ times better than 3GPP Release 6 (HSPA);

- Throughput: Target for average user throughput per MHz is $3 - 4$ and $2 - 3$ times better than HSPA for downlink and uplink respectively;

- Very low latency: Short setup time and Short transfer delay, Control-plane latency $< 50 - 100$ msec and User-plane latency < 10 msec;

- Support of variable bandwidths: 1.4, 3, 5, 10, 15, and 20 MHz;

- Support of FDD and TDD within a single radio access technology;

- Simplified, flat network architecture;

- Enhanced Multimedia Broadcast Multicast Services (E-MBMS): MBMS shall be further enhanced and will be referred to as E-MBMS;

- Quality of Service: End-to-end Quality of Service (QoS) shall be supported. VoIP should be supported with at least as good radio and backhaul efficiency and latency as voice traffic over the UMTS circuit switched networks;

- High mobility: Providing optimal performance up to 15 km/h and maintaining connectivity with users that move up to 350 km/h;

- Advanced MIMO spatial multiplexing techniques: 4×2, 2×2, 1×2, 1×1 and 1×2, 1×1 are the supported antenna configurations for downlink and uplink respectively. Multi-user MIMO is also being considered.

- Compatibility and inter-working with earlier 3GPP Releases;

- Co-existence with legacy standards: Users can transparently start a call or transfer of data in an area using an LTE standard, and, when there is no coverage, continue the operation without any action on their part using GSM/GPRS or W-CDMA-based UMTS;

- Cost efficiency: Reduced CAPital and OPerational EXpenditure (CAPEX, OPEX), and cost effective migration from legacy networks.

2.3 LTE Physical Layer Description

The design of the LTE physical layer (PHY) is very much influenced by requirements for high peak transmission rate, spectral efficiency, and variable channel bandwidths. In this section, the main functional element of the LTE physical layer processing, defined in the 3GPP specifications [6, 11, 12] are discussed.

2.3.1 Multiple Access Schemes

LTE uses asymmetric multiple access schemes in the downlink and uplink. The multiple access scheme in the downlink is based on OFDMA, and for the uplink LTE specifies SC-FDMA. OFDMA, due to its multi-carrier nature, is compatible for achieving high peak data rates in high spectrum bandwidth. On the uplink, however, a pure OFDMA approach results in high PAPR of the signal, which leads to low power efficiency. Hence, LTE uses SC-FDMA as the multiple access scheme for uplink, which is somewhat similar to OFDMA but is much more power efficient.

2.3.2 Operating Frequencies and Bandwidths

The bandwidth capability of an LTE-compliant UE (User Equipment) is much higher than that of previous 3GPP releases, enabling much higher throughput and peak data rates in the downlink and uplink. Scalable bandwidth is one of the most important properties of LTE. The amount of bandwidth in an LTE system can be scaled from 1.4 to 20 MHz as opposed to the fixed 5 MHz channels that WCDMA/HSPA uses. This means networks can be launched with a small amount of spectrum, alongside existing services, and more spectrum can be added as users switch over. Besides, the scalable bandwidth of LTE will allow operators to easily migrate their networks and users from HSPA to LTE over time.

2.3.3 Modulation and Coding

The baseband modulation schemes supported in LTE are Quadrature Phase Shift Keying (QPSK), 16QAM (Quadrature Amplitude Modulation), and 64QAM. For channel coding, LTE uses turbo and convolutional codes [11]. The turbo encoder scheme specified for LTE is a Parallel Concatenated Convolutional Code (PCCC) with two eight-state constituent encoders and one turbo code internal interleaver, and the coding rate is 1/3. The convolutional code specified in LTE also has a rate of 1/3 and is a tail biting convolutional code with a constraint length of 7 and generator matrix [133 171 165] (octal representation).

2.3.4 Frame Structure

Downlink and uplink transmissions are organized into radio frames of 10 ms duration. Each 10 ms frame is divided into 10 equally sized subframes. LTE supports two types of frame structures; Type 1 is for FDD (Frequency Division

Duplex) transmissions and Type 2 is applicable for TDD (Time Division Duplex) transmissions [12].

Frame structure Type 1 is shown in Fig. 2.1. Each subframe consists of 2 equally sized slots, where each slot has a duration of 0.5 ms. 20 slots, numbered from 0 to 19, constitute 1 radio frame. The 1 ms duration of a subframe is an LTE *Transmission Time Interval* (TTI). For FDD, 10 subframes are available for downlink transmission and 10 subframes are available for uplink transmission in each radio frame. Uplink and downlink are separated in the frequency domain.
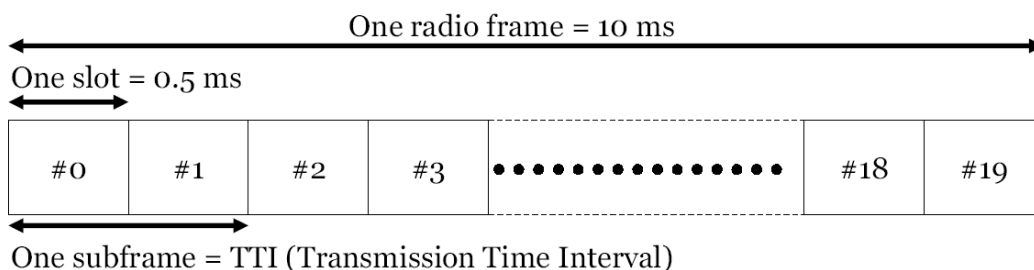
Figure 2.1. Structure of Type 1 frames [12].

Frame structure Type 2 is shown in Fig. 2.2. For TDD, uplink and downlink transmissions share the same frequency band. Each 10 ms radio frame consists of 2 half-frames of 5 ms (5 subframes) each. In each half-frame, 4 of the 5 subframes carry physical channels. Subframe 0 and 5 always carry downlink physical channels. The other frames can carry either uplink or downlink physical channels. Subframes 1 and 6 carry synchronization signals. Each half-frame consists of 8 slots of 0.5 ms length and 3 special field: downlink pilot time slot (DwPTS), guard period (GP), and uplink pilot time slot (UpPTS). Subframe 1 and 6 always contain GP and either DwPTS or UpPTS depending on the direction of transmission of the physical channels in the other subframes.

One radio frame = 10 ms

One half-frame = 5 ms

One subframe = 1 ms

One slot = 0.5 ms

| Subframe #0 | | | Subframe #2 | Subframe #3 | Subframe #4 | Subframe #5 | | | Subframe #7 | Subframe #8 | Subframe #9 |

DwPTS   GP   UpPTS   DwPTS   GP   UpPTS
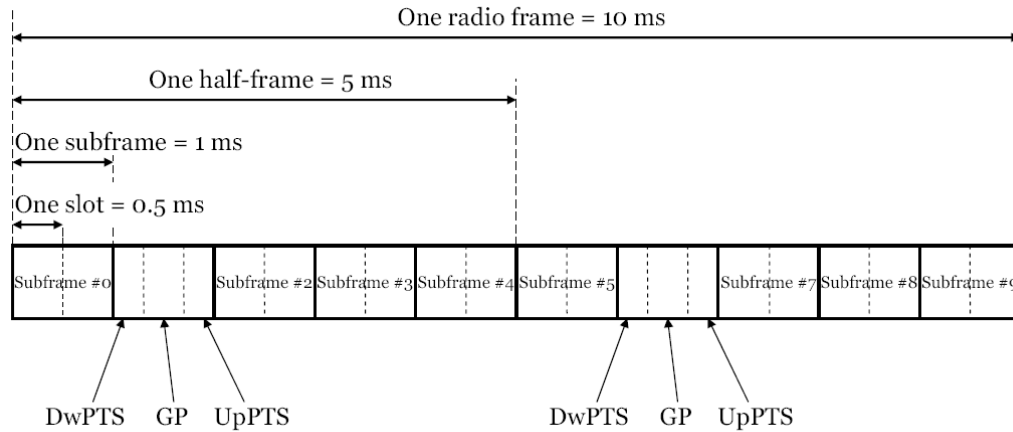
Figure 2.2. Structure of Type 2 frames [12].

2.3.5 Physical Resource Blocks

In LTE, transmission resources are assigned to physical channels in time-frequency units called Resource Blocks (RB). The smallest time-frequency unit used for downlink/uplink transmissions is called a resource unit or resource element. A resource unit is defined as one subcarrier over one symbol. A group of 12 subcarriers contiguous in frequency over one slot (0.5 ms) in time domain form a resource block, for both TDD and FDD systems as well as in both uplink and downlink. Each subcarrier has a spacing of 15 KHz and the total bandwidth that one resource block occupies is 180 KHz for 12 subcarriers. A physical channel occupies a frequency band containing one or more contiguous resource blocks. The bandwidth of a physical channel is a multiple of 180 KHz. All the resource blocks in the available bandwidth constitutes a resource grid. There are 6, 15, 25, 50, 75 and 100 resource blocks corresponding to 1.4, 3, 5, 10, 15, and 20 MHz channel bandwidths respectively. Figure 2.3 shows the generic resource block and grid structure for uplink/downlink. The number of subcarriers and symbols

per resource block is denoted by N_{sc}^{RB} and N_{symb} respectively and the number of resource blocks in a resource grid is denoted by N_{RB}.
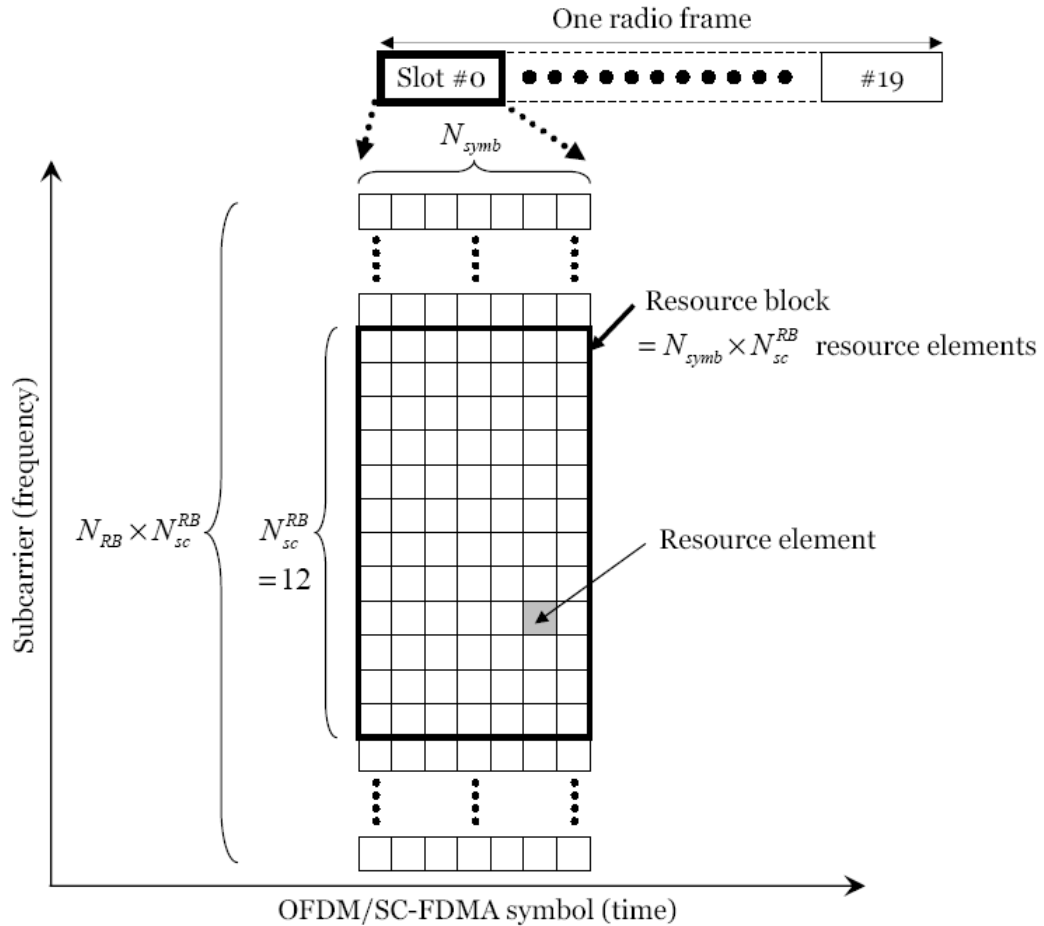
Figure 2.3. Resource Block structure [12].

2.3.6 Cyclic Prefix

Each slot in the time domain carries three (only for downlink), six or seven symbols. One symbol contains the complex outputs of one IDFT operation. In LTE, the complex numbers produced by the IDFT operation and the complex numbers in the cyclic prefix are referred to as *samples*. LTE uses slots with six

symbols in large cells, which are subject to severe intersymbol interference because of long multipath delay spread and seven symbols in smaller cells. The CP length is chosen to be longer than the maximum delay spread in the channel. The number of symbols per slot and the selected CP length for LTE is shown in Table 2.1. As can be seen in Table 2.1, there are two (three for downlink) different CP lengths: normal CP is used in smaller cells with seven symbols per slot and extended CP is required for cells with six or three symbols (only for downlink) per slot.

CP configuration	CP length	No of symbols per slot
Normal CP	5.21 (first symbol of the slot)	7
	4.69 (other symbols of the slot)	
Extended CP	16.67 (all symbols of the slot)	6
Extended CP	33.33 (all symbols of the slot)	3

Table 2.1. Cyclic Prefix Length and Number of symbols per slot [3].

The basic transmission parameters of LTE are specified in Table 2.2. It can be observed from Table 2.2 that the size of the IDFT for each channel bandwidth is larger than the number of occupied subcarriers. The remaining subcarriers in the bandwidth have zero magnitude and constitute a guard band in the frequency domain to prevent out-of-band radiation.

Channel Bandwidth (MHz)	1.4	3	5	10	15	20
Number of RBs	6	15	25	50	75	100
Number of occupied subcarriers	72	180	300	600	900	1200
IDFT(Tx)/DFT(Rx) size	128	256	512	1024	1536	2048
Sample rate [MHz]	1.92	3.84	7.68	15.36	23.04	30.72
Samples per slot	960	1920	3840	7680	11520	15360

Table 2.2. Transmission Parameters of LTE [3, 6].

Chapter 3

SC-FDMA Fundamentals

SC-FDMA is a multiple access scheme that has recently gained popularity because of its power efficiency and has been selected for uplink LTE. It is a variant of the Orthogonal Frequency Division Multiple Access (OFDMA). OFDMA is the multi-user version of OFDM. Similarly SC-FDMA is the multi-user version of SC-FDE (Single Carrier modulation with Frequency Domain Equalization). To explain how an SC-FDMA system works, we first discuss the basics of OFDM and its similarity with SC-FDE. Afterwards, we describe their multiple user version, OFDMA and SC-FDMA, and compare the transmitter and receiver structure. A good reference on the subject of single carrier modulation is [3] and the interested reader is referred there for additional information on the topics covered in this Chapter.

3.1 SC-FDE and OFDM

OFDM is a multi-carrier modulation scheme that uses groups of orthogonal subcarriers to carry data. In an OFDM system, the input bit stream is divided

into many parallel bit streams with each stream modulating a subcarrier. In recent years, OFDM has become the modulation method of choice for many wireless technologies due to the numerous advantages it offers, including robustness against interference in frequency selective multipath channels, simple method of equalization, and the ability to handle very high data rates.

Despite its many advantages, however, OFDM has a major drawback: low power efficiency. OFDM waveforms exhibit pronounced envelop fluctuations resulting in a very high PAPR. For signals with a large PAPR, highly linear power amplifiers are required to avoid excessive inter-modulation distortion. In order to make sure the power amplifier operates in the linear region, they have to operate with a large back-off (must be at least equal to the PAPR) from their peak power. If the input power is not backed off, signal distortion occurs. This results in out-of-band spectral regrowth and leads to low power efficiency in the power amplifier. Because of this, numerous techniques have been developed to reduce OFDM PAPR. SC-FDE is one outcome of such investigations.

SC-FDE and OFDM has similar components in their structure as shown in Fig. 3.1.
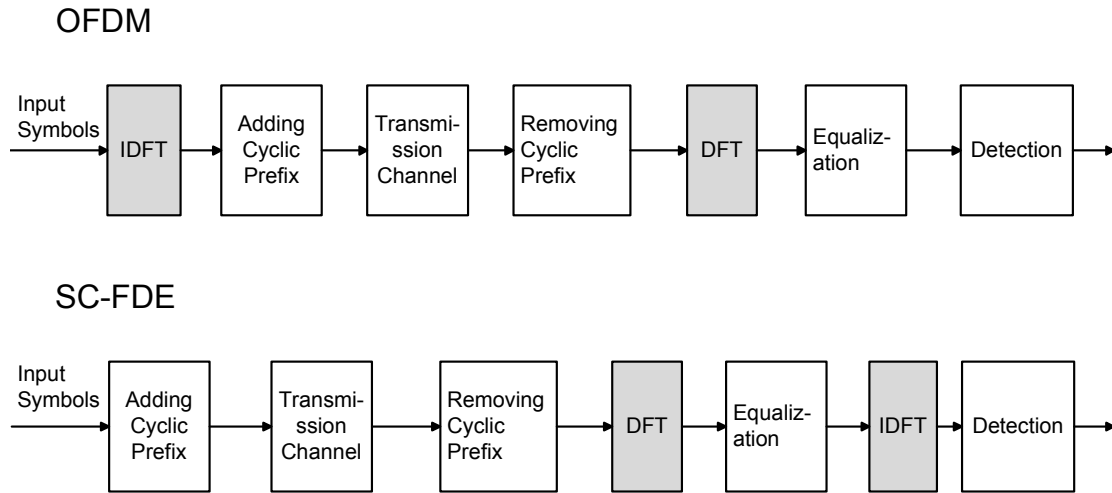
OFDM

SC-FDE

Figure 3.1. Block diagrams of OFDM and SC-FDE systems [3].

Comparing the systems in Fig. 3.1, SC-FDE and OFDM have the same communication blocks; the only difference is the locations of the DFT and IDFT blocks (gray colored blocks in Fig. 3.1). Because of the single carrier modulation at the transmitter, SC-FDE does not have the high PAPR disadvantage as OFDM. Also it has other advantages over OFDM, such as: robustness to spectral null, lower sensitivity to carrier frequency offset, and lower complexity at the transmitter.

3.2 SC-FDMA and OFDMA

SC-FDMA is based on the same principle as SC-FDE, the only difference is SC-FDMA is for multiple users, whereas SC-FDE is a single-user modulation scheme. The system configuration in an SC-FDMA system is similar to OFDMA with the addition of a DFT and an IDFT block. Figures 3.2 and 3.3 show the generic structures of OFDMA and SC-FDMA respectively.
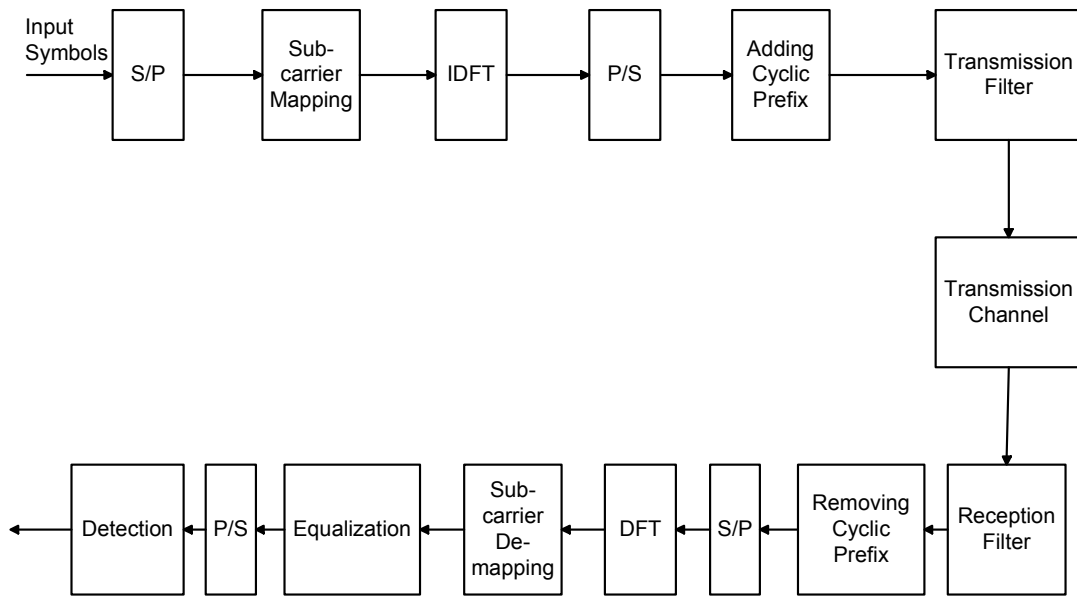
Figure 3.2. Block diagram of an OFDMA system [3].
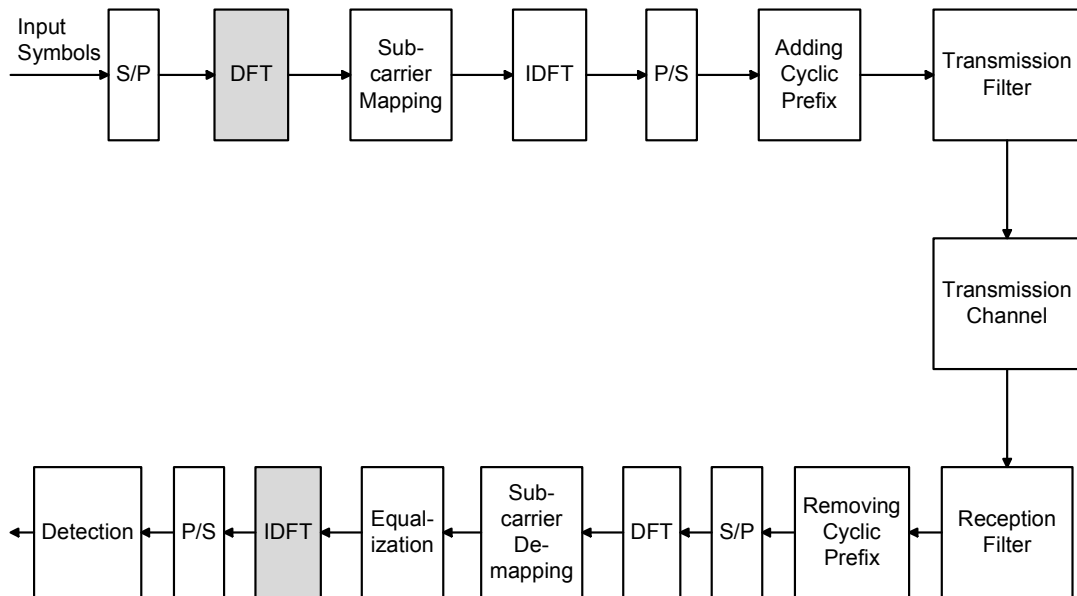
Figure 3.3. Block diagram of an SC-FDMA system [3].

Figures 3.2 and 3.3 show that the only difference between an OFDMA and an SC-FDMA system is the two additional DFT/IDFT blocks in the SC-FDMA sys-

tem, shown in gray color in Fig 3.3. For this reason, SC-FDMA is also referred to as DFT-precoded or DFT-Spread OFDMA. Although the communication blocks in the two systems are similar, the two systems perform differently. In OFDMA, the input information bits corresponding to each user are converted to symbols (complex numbers) by means of a modulation method, and the generated symbols are assumed to be in the frequency domain. The symbols are then mapped to a distinct set of subcarriers. The IDFT block converts the symbols into the time domain, which are then transmitted though the channel after adding the cyclic prefix. The IDFT operation can be viewed as each symbol modulating one subcarrier and transmitting the subcarriers in parallel.

On the other hand, in SC-FDMA, the generated symbols are assumed to be in the time domain. The additional DFT operation in the transmitter spreads the energy of each symbol over the whole group of subcarriers. In other words, each subcarrier carries a portion of the information conveyed by each symbol. The subcarriers are then transmitted sequentially rather than in parallel. It is the parallel transmission of subcarriers that gives rise to the high PAPR in OFDMA, and SC-FDMA obtains the advantage of low PAPR because of sequential transmission of subcarriers.

On the receiver side, frequency domain equalization is done in OFDMA on a per-subcarrier basis, whereas in SC-FDMA it is done by using a complex equalizer used for all the subcarriers together. The receiver structure is therefore complex in SC-FDMA compared to OFDMA. However, on the transmitter side, the low PAPR advantage allows the use of simple power amplifiers that reduces the power consumption. This makes SC-FDMA more suitable for uplink transmission, where the receiver is placed in the base station and transmitter is at the mobile station,

since power efficiency and complexity are more important for mobile stations than in the base stations.

3.3 SC-FDMA Transmitter

In a typical SC-FDMA transmitter, the DFT and the IDFT are the two major computations required to generate the single carrier FDMA signal. The SC-FDMA transmitter first converts the input information bit stream into a parallel bit stream, then it groups the bits into sets of m bits, and the sets are mapped to M-ary symbols where $M = 2^m$. The DFT block operates on chunks of symbols with each chunk containing K symbols. A K point DFT operation transforms the time domain symbols into the frequency domain. Next, the transmitter maps the outputs of the DFT block to N_{total} orthogonal subcarriers where $N_{\text{total}} > K$. In a system with J user terminals, if all the terminals transmit K symbols per block, then $N_{\text{total}} = K \times J$. After subcarrier mapping, an N_{total} point Inverse DFT (IDFT) operation is performed to generate a time domain signal. The transmitter then adds the Cyclic Prefix (CP), containing the last part of the block of symbols, to the start of the block in order to prevent against Inter Block Interference (IBI). Finally, after passing through the transmission filter for pulse shaping, the signal is transmitted.

3.4 Subcarrier Mapping

There are two types of subcarrier mapping in an SC-FDMA system, localized (LFDMA) and distributed (DFDMA). In LFDMA, the K outputs of the DFT block from a particular terminal are mapped to a chunk of K adjacent sub-

carriers, whereas in DFDMA the symbols are mapped to subcarriers which are equally spaced across a particular part of the (or the entire) bandwidth. Interleaved SC-FDMA (IFDMA) is a special case of DFDMA, where the chunk of K subcarriers occupy the entire bandwidth with a spacing of $J - 1$ subcarriers. In both of the subcarrier allocation methods, the transmitter assigns zero amplitudes to the remaining $N_{\text{total}} - K$ unused subcarriers. Figure 3.4 illustrates the different types of subcarrier mapping methods.
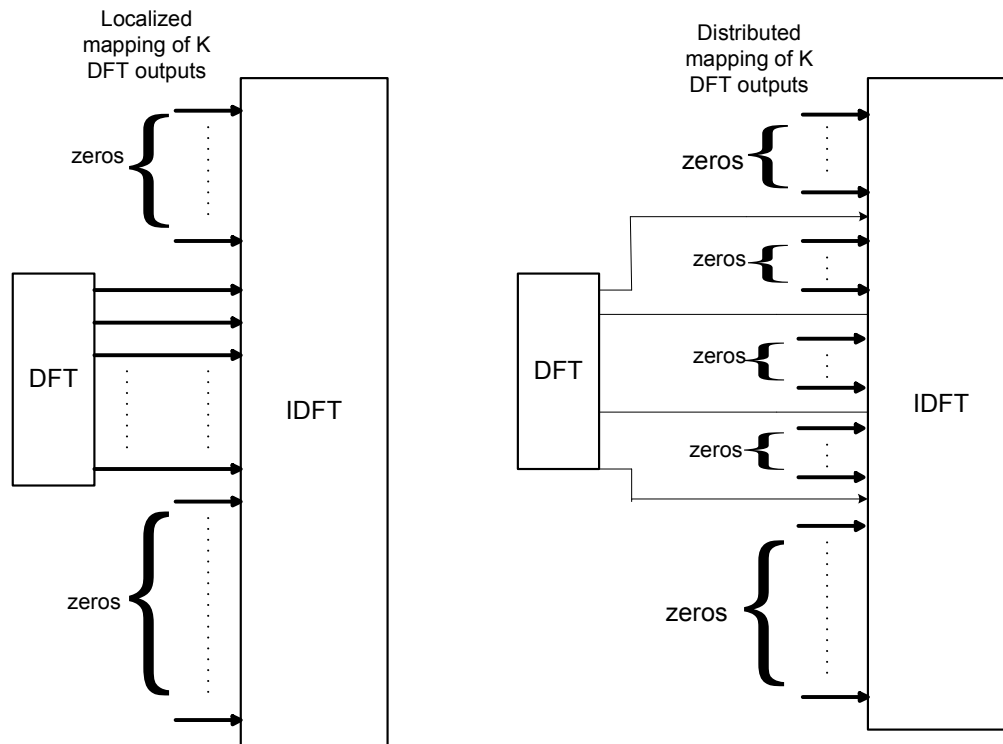
Figure 3.4. Localized and Distributed subcarrier mapping.

Figure 3.5 demonstrates an example of the two different SC-FDMA subcarrier mapping method, for $K = 3$ symbols per block, $N_{\text{total}} = 9$ subcarriers, and $J = 3$ user terminals. The input time domain symbols from user terminal J_0 are u_0, u_1, and u_2, and U_0, U_1, and U_2 represent the outputs of the DFT blocks.

In localized mapping, outputs of the DFT blocks will occupy the subcarriers $0, 1,$ and 2, and the rest of the subcarriers will have zero amplitudes. In a similar manner the DFT outputs from user J_1 and J_2 will each occupy 3 subcarriers, starting with subcarrier number 3 and 6, respectively. In the Interleaved mapping, the DFT outputs from terminal J_0 will be uniformly distributed among the 9 subcarriers starting with the 0th one, and $3 - 1 = 2$ zeros will be assigned to the subcarriers in between the occupied ones. Similarly, the DFT outputs from user terminal J_1 and J_2 will each occupy 9 equally spaced subcarriers starting with subcarrier number 1 and 2, respectively. Only the subcarrier allocation for user terminal J_0 is shown in Fig 3.5.
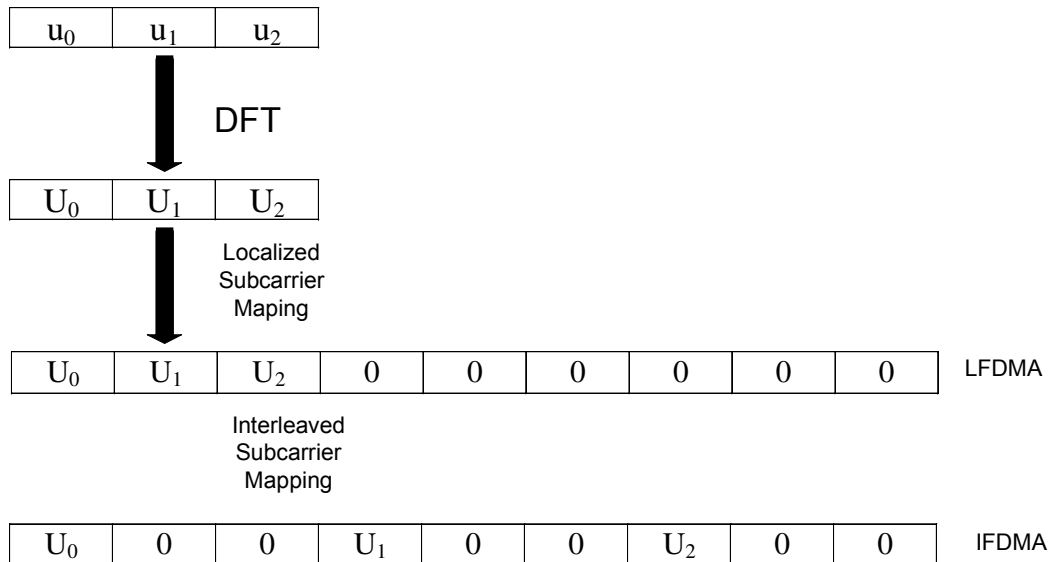
Figure 3.5. An example of localized and interleaved subcarrier mapping method.

3.5 Time Domain Representation of SC-FDMA Signals

In an IFDMA transmitter, the time domain signal that is obtained after the DFT and IDFT operations consists of the actual input symbols, which are repeated J times and scaled by a factor of $1/J$. The symbols are also phase rotated, which is done by multiplying each symbol by a factor of $\exp(j2\pi il/N_{\text{total}})$, where i denotes the user terminal location, l is the output sample number in the time domain, and N_{total} is the size of the IDFT. In the example shown in Fig. 3.5, the time domain symbols will be the input symbols, scaled by a factor of $1/3$, phase rotated by $\exp(j2\pi il/9)$ where $i = 0, 1, 2, \; l = 0, 1, 2, \ldots, 8$, and repeated 3 times. The time domain samples of IFDMA, denoted by v_l, are expressed as

$$v_l = \frac{1}{J} u_{(l)\bmod \text{K}} \cdot e^{j2\pi \frac{il}{N_{\text{total}}}} \tag{3.1}$$

In LFDMA, the time domain signal has copies of input time symbols with a scaling factor of $1/J$ at sample positions that are integer multiples of J, and the $N_{\text{total}} - K$ time samples are weighted sums of all the symbols in the block. The time domain representations of LFDMA is shown in (3.2) [3]. Detail derivation of (3.1) and (3.2) can be found in [3] and are also provided in Appendix A.

$$v_l = v_{Jr+p} = \begin{cases} \frac{1}{J} u_{(l)\bmod \text{K}}, & p = 0 \\ \frac{1}{J}\left(1 - e^{j2\pi\frac{p}{J}}\right) \frac{1}{K} \sum_{s=0}^{K-1} \frac{u_s}{1 - e^{j2\pi\left\{\frac{r-s}{K} + \frac{p}{JK}\right\}}}, & p \neq 0 \end{cases} \tag{3.2}$$

where $0 \leq r \leq K - 1$ and $0 \leq p \leq J - 1$. For both IFDMA and LFDMA, each transmitted symbol has a duration of $\frac{1}{J}$ times the duration of the input symbols. The time domain representation of LFDMA and IFDMA signals are shown in Fig 3.6 for the example demonstrated in Fig. 3.5.

Input symbols

u_0	u_1	u_2

Time domain
symbols of
IFDMA

u_0	u_1	u_2	u_0	u_1	u_2	u_0	u_1	u_2

$\times \dfrac{1}{J}$

Time domain
symbols of
LFDMA

u_0	c_0	c_1	u_1	c_2	c_3	u_2	c_4	c_5

$\times \dfrac{1}{J}$
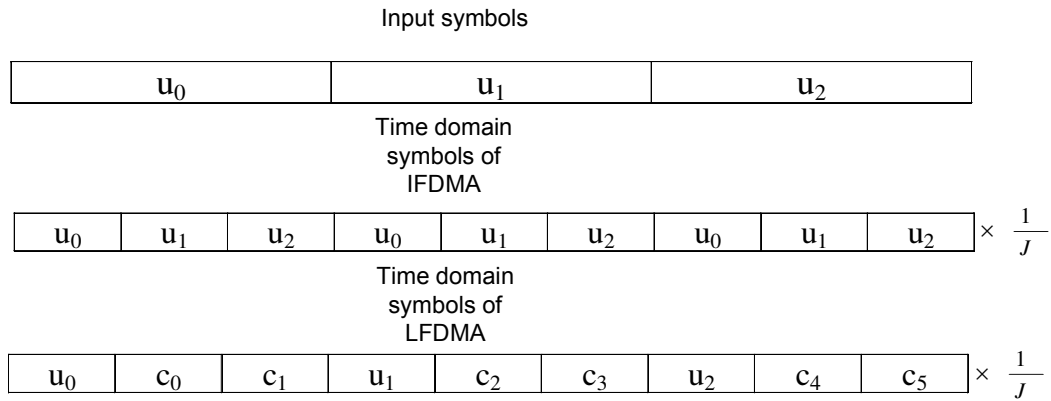
c_i, $i = 0, 1, 2 \ldots\ldots$ denotes
complex weighted sum of the
input symbols, u_0, u_1, $\ldots\ldots$

Figure 3.6. Time Domain Representation of IFDMA and LFDMA.

3.6 Comparison of Different Subcarrier Mapping Methods

The different versions of SC-FDMA with different subcarrier allocation methods vary in their properties such as: power efficiency, performance in frequency selective channels, and system throughput. The PAPR is a useful metric for measuring the power efficiency of a transmission scheme. The PAPR (in dB) of a continuous-time signal, $x(t)$ can be defined by the following equation [3]

$$
\begin{aligned}
\text{PAPR} &\triangleq \frac{\text{peak power of } x(t)}{\text{average power of } x(t)} \\
&\triangleq 10\log_{10}\left(\frac{\max\limits_{0 \leq t \leq KT} |x(t)|^2}{\frac{1}{KT}\int_0^{KT} |x(t)|^2 dt} \right) \quad \text{(in dB)}
\end{aligned}
\tag{3.3}
$$

where, $x(t)$ represents the transmitted signal in the time domain, K is the number of symbols, T is the symbol duration, and KT represents the signal duration.

As (3.1) and (3.2) show, the time domain samples in IFDMA consist of the

actual input symbols only, whereas in LFDMA they also include the complex-weighted sum of all the input symbols in the block. Therefore, the transmitted waveforms in LFDMA have more amplitude fluctuations than in IFDMA. As a result, LFDMA has much higher PAPR compared to IFDMA. Detailed analysis on PAPR of SC-FDMA signals can be found in [13].

In frequency selective channels, where the channel gain is not constant over the entire bandwidth, LFDMA has worse performance than IFDMA. Since in IFDMA the data is distributed throughout the whole bandwidth, it is not affected by the channel gain. The error performance will be the same for all users. But in LFDMA, each user utilizes a block of subcarriers located at a particular area of the total bandwidth, so the bit error rate will vary from one user to another depending on where the block of the subcariers is located.

To improve the performance of LFDMA schemes in frequency selective channels, channel-dependent subcarrier allocation (CDS) instead of static (round robin) scheduling can be used. Channel dependent scheduling is a form of subcarrier mapping, where the transmission of each terminal is mapped to a set of subcarriers with favorable transmission characteristics. Myung and Goodman in [14], showed that when CDS is applied, there is a significant improvement in the average throughput for both IFDMA and LFDMA. But compared to IFDMA, the capacity gain from CDS is much higher in LFDMA. Therefore, as discussed in [14], when power efficiency is considered, IFDMA is more desirable than LFDMA, but in terms of system throughput, LFDMA outperforms IFDMA when CDS is applied.

3.7 SC-FDMA Receiver

Just like the transmitter, the two major computations required to get back the transmitted symbols in an SC-FDMA receiver are the DFT and IDFT. In an SC-FDMA receiver, after discarding the cyclic prefix, the DFT block transforms the received time domain signal into the frequency domain. Afterwards, subcarrier de-mapping is done following the same method (distributed, localized or interleaved) in which subcarrier mapping was done in the transmitter. Next, an equalizer compensates for the distortion caused by the multipath propagation channel. After the equalization process, the IDFT block transforms the signal into the time domain, and finally, a detector recovers the original transmitted symbols.

The equalization process in an SC-FDMA receiver is done in the frequency domain. Frequency domain equalization is one of the most important properties of SC-FDMA technology. Conventional time domain equalization approaches for broadband multipath channels are not advantageous because of the complexity and required digital signal processing increases with the increase of the length of the channel impulse response. Frequency domain equalization, on the other hand, is more computationally efficient and therefore desirable because the DFT size does not grow linearly with the length of the channel impulse response. Most of the time domain equalization techniques such as MMSE (Minimum Mean Squared Error Equalization), DFE (Decision Feedback Equalization), and turbo equalization can be implemented in the frequency domain.

Chapter 4

CPM-SC-FDMA Signal Model

CPM is a phase modulation scheme, where the phase of the carrier signal is varied in a continuous manner. In this section, we first discuss the basics of CPM, the modulation method that we are applying to the SC-FDMA multiple access scheme, and then we provide the details of the CPM-SC-FDMA signal model.

4.1 CPM Basics

The two most important properties of CPM are its constant envelope and continuous phase. The constant envelop property of CPM results from the information being carried only by the phase of the carrier signal; there is no variation in the amplitude of the signal. Constant envelop signals allow the power amplifier that the mobile system uses to operate near saturation without distorting the signal. This is required for achieving high power efficiency, because power amplifiers are most efficient when they are driven into saturation.

The continuous phase property of CPM results in high spectral efficiency. In modulation schemes such as BPSK, QPSK, and 8PSK, there are abrupt changes

in the phase of the carrier signal at symbol transitions. The phase discontinuity in the carrier signal causes out-of-band radiation, leading to poor spectral efficiency. Because of its superior spectral performance and higher power efficiency, CPM is preferred over most other phase modulation schemes.

A CPM waveform is described by the following equation [15]

$$s(t; \boldsymbol{\beta}) \triangleq \exp\{j\phi(t; \boldsymbol{\beta})\} \tag{4.1}$$

where ϕ is the phase of the signal given by

$$\phi(t; \boldsymbol{\beta}) \triangleq 2\pi \sum_i \beta_i h_i q(t - iT). \tag{4.2}$$

Here, $\boldsymbol{\beta} \triangleq \{\beta_i\}$ represents the discrete time symbol sequence of M-ary data symbols with each symbol carrying $m = \log_2 M$ bits. h_i is the modulation index, which determines the total amount of phase change at the appearance of a symbol. The value of h_i may vary from one symbol interval to another, and this is termed as multi-h CPM. For this work, however, we will only consider single-h CPM schemes; that is, h_i having a constant value, h, throughout all symbol intervals. We assume that h can be represented as a rational number and is defined as

$$h = \frac{k}{p} \tag{4.3}$$

where k and p are two mutually prime integers. The *phase response function* is represented by $q(t)$, which is obtained by integrating the *frequency response function*, $g(t)$. Shape of $g(t)$ determines the smoothness of phase change. The length of $g(t)$ is denoted by L in units of symbol intervals (T). If $L = 1$; i.e,

$g(t)$ has a duration of one symbol interval, the signal is called *full-response* CPM. Furthermore, if $L > 1$; i.e, $g(t)$ has a duration longer than one T, the modulated signal is called *partial-response* CPM. Rectangular (LREC), Raised Cosine (LRC) and Gaussian are some pulse shapes generally used for $g(t)$ and are defined in (4.4), 4.5, and 4.6 respectively.

$$g_{\text{LREC}}(t) = \begin{cases} \frac{1}{2LT}, & 0 \leq t \leq LT \\ 0, & \text{otherwise.} \end{cases} \tag{4.4}$$

$$g_{\text{LRC}}(t) = \begin{cases} \frac{1}{2LT}\left[1 - \cos\left(\frac{2\pi t}{LT}\right)\right], & 0 \leq t < LT \\ 0, & \text{otherwise.} \end{cases} \tag{4.5}$$

$$g_{\text{GMSK}}(t) = \frac{1}{2T}\left[Q\left(\frac{\frac{t}{T}+\frac{1}{2}}{\sigma}\right) - Q\left(\frac{\frac{t}{T}-\frac{1}{2}}{\sigma}\right)\right] \tag{4.6}$$

where

$$Q(t) = \int_t^\infty \frac{1}{\sqrt{2\pi}}e^{\frac{-x^2}{2}}dx \tag{4.7}$$

$$\sigma^2 = \frac{\ln 2}{4\pi^2(BT)^2}. \tag{4.8}$$

Here, BT is the *time-bandwidth product*.

The phase response function, $q(t)$ can be expressed by the following equation

$$q(t) = \begin{cases} 0, & t < 0 \\ \int_0^t g(\tau)d\tau, & 0 \leq t < LT \\ \frac{1}{2}, & t \geq LT. \end{cases} \tag{4.9}$$

The phase, $\phi(t; \boldsymbol{\beta})$, is obtained by passing the frequency signal through an inte-

grator, where the frequency signal is given by

$$f(t; \boldsymbol{\beta}) = h \sum_{i=n-L+1}^{n} \beta_i g(t - iT). \tag{4.10}$$

The frequency response function, $g(t)$, modulation index, h, and alphabet size, M are the basic parameters that define a CPM scheme. By varying these parameter an infinite number of CPM schemes can be obtained.

The phase, $\phi(t; \boldsymbol{\beta})$, can be decomposed into two parts

$$\phi(t; \boldsymbol{\beta}) = 2\pi h \sum_{i=n-L+1}^{n} \beta_i q(t - iT) + \pi h \sum_{i=-L+1}^{n-L} \beta_i$$

$$= \theta(t; \boldsymbol{\beta}) + \theta_n. \tag{4.11}$$

The first term, $\theta(t; \boldsymbol{\beta}_n)$, is a function of the *correlative state vector*, which is defined as

$$\boldsymbol{\beta} \triangleq \{\beta_{n-L+1}, \dots, \beta_{n-1}, \beta_n\}. \tag{4.12}$$

Each of the L symbols in $\boldsymbol{\beta}_n$ can have M values, and the correlative state vector can have a total of M^L values. The second term, θ_n, is the phase state. Since the modulation index, h $(= \frac{k}{p})$, is assumed to be rational, the phase state, when taken modulo-2π, can have exactly p values if k is even and $2p$ values if k is odd, which are uniformly spaced around the unit circle; i.e,

$$\theta_n = \left\{ 0, \frac{\pi k}{p}, \frac{2\pi k}{p}, \dots, (p-1)\frac{\pi k}{p} \right\} \tag{4.13}$$

when k is even and

$$\theta_n = \left\{0, \frac{\pi k}{p}, \frac{2\pi k}{p}, \ldots, (2p-1)\frac{\pi k}{p}\right\} \tag{4.14}$$

when k is odd.

Thus, a CPM signal can be represented by a phase trellis. The number of states and branches in a CPM trellis are determined by the values of p, M, and L.

$$\text{Number of states, } N_s = \begin{cases} pM^{L-1}, & k \text{ even} \\ 2pM^{L-1} & k \text{ odd} \end{cases} \tag{4.15}$$

$$\text{Number of branches, } N_B = \begin{cases} pM^{L}, & k \text{ even} \\ 2pM^{L} & k \text{ odd.} \end{cases} \tag{4.16}$$

4.1.1 CPM Parameters

In this section, we present a brief review on how different parameters affect the performance of a CPM scheme. A detailed analysis on this topic can be found in [15–18].

Performance of a CPM scheme is dependent on the choice of the following parameters:

- Alphabet size, M;

- modulation index, h;

- Frequency pulse, $g(t)$ and

- Length of $g(t)$, L.

These parameters effect two aspects of performance:

- Spectral performance and

- Error performance.

The spectral performance of a CPM scheme is determined by two factors, width of the main lobe and sidelobe decay level. Most of the time there is a trade-off between these two factors.

Effect of varying M and h on the spectral performance of a CPM signal are shown in Fig. 4.1, and 4.2, respectively. Fig 4.3 shows the average PSD of a CPM signal for Rectangular (REC), Raised Cosine (REC) and Gaussian frequency pulse. Effect of varying the length of the frequency pulse is shown in Fig. 4.4. In Figs. 4.1 to 4.4, effect of different parameters on the CPM spectrum is demonstrated by plotting the average PSD (Power Spectral Density) of a CPM signal for different values of a particular parameter while keeping the other parameters constant.
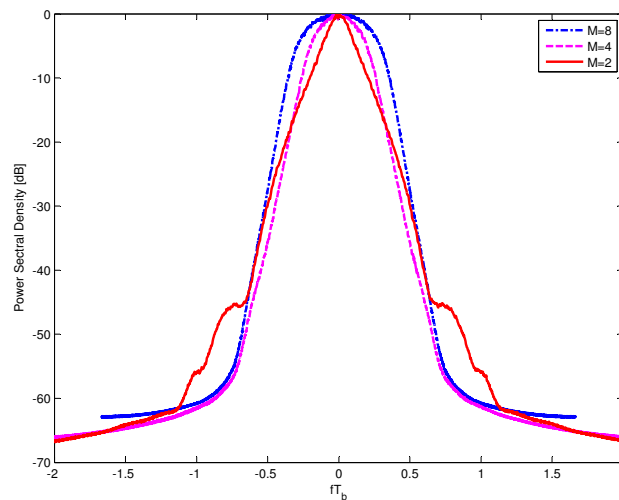
Figure 4.1. Effect of varying the alphabet size, M on CPM spectrum. Parameters of the CPM scheme: $L = 3$, RC, $h = 5/16$
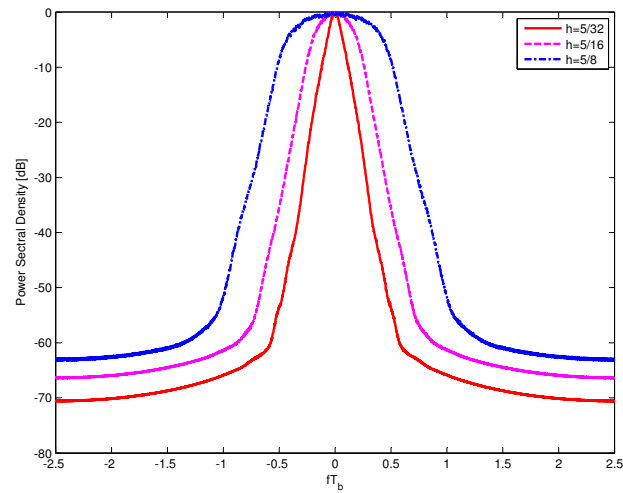
Figure 4.2. Effect of varying the modulation index, h on CPM spectrum. Parameters of the CPM scheme: $L = 3$, RC, $M = 4$
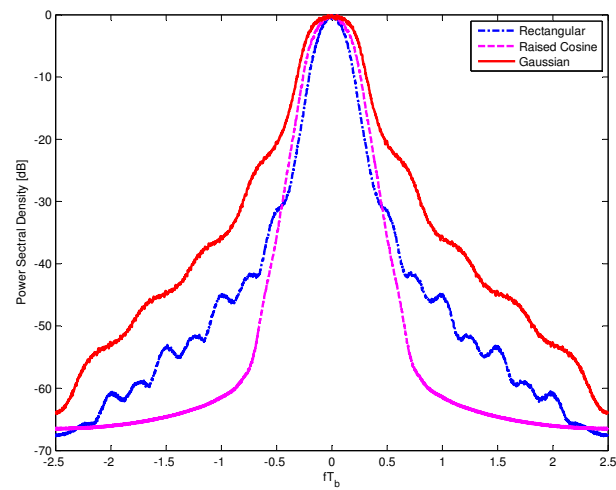
Figure 4.3. CPM spectrum for different frequency pulses, $g(t)$. Parameters of the CPM scheme: $L = 3$, $M = 4$, $h = 5/16$
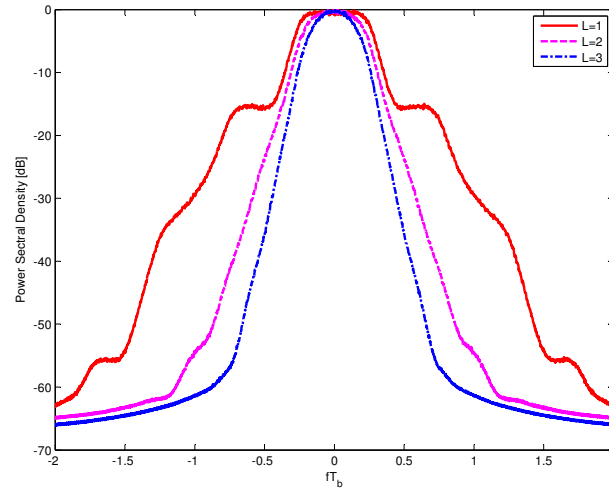
Figure 4.4. Effect of varying the pulse length (L) on CPM spectrum. Parameters of the CPM scheme: RC, $M = 4$, $h = 5/16$

If bandwidth is defined at a sidelobe decay level of -20 dB, then it can be seen from Fig 4.1 that increasing M increases the bandwidth. but at lower decay level, increasing M gives more compact spectrum. Increasing h on the other hand, results in poor spectral performance as shown in Fig. 4.2. Fig. 4.3 shows that the scheme with the RC frequency pulse has a narrower spectrum and lower sidelobes than the one with the REC pulse. Increasing the length of the frequency pulse however, increases the spectral efficiency, for any frequency pulse, as shown in Fig. 4.4.

The error performance of a CPM scheme depends on the minimum squared Euclidean distance, $d_{\min}^2$. The probability of symbol error for CPM is given by the following equation

$$P_e \approx Q\left(\sqrt{\left(d_{\min}^2 \frac{E_b}{N_0}\right)}\right) \tag{4.17}$$

where

$$d_{\min}^2 \equiv \frac{1}{2E_b} \min_{p,r,p \neq r} \int \left(s_p(t) - s_r(t)\right)^2 dt. \tag{4.18}$$

Here, $s_p(t)$ and $s_r(t)$ represent two transmitted signals, E_b is the energy per bit and N_0 is the noise PSD. From Equation 4.17 it is evident that the scheme with a higher $d_{\min}^2$ will have a lower probability of error. d_B^2, the upper bound of $d_{\min}^2$, is a useful metric for determining the error performance of a CPM scheme. A detailed analysis on computing the value of d_B^2 can be found in [15, Chapter 3], where it was shown that for a particular h, larger L and M yield schemes with higher minimum distance and therefore better error performance. It was also shown in [15] that there is no single frequency pulse that is uniformly good for all CPM schemes, in terms of error performance. A particular frequency pulse may yield good error performance for lower values of h, but the same may not happen for larger values of h. So for choosing $g(t)$, spectral performance should be considered.

Choosing the right parameters for a CPM scheme is important for its application. For finding which CPM scheme is more bandwidth efficient, the PSD plots of different CPM schemes can be utilized. For error performance, however, finding $d_{\min}^2$ is the only way to determine the error performance of a CPM scheme. In [15], plots of d_B^2 with respect to modulation index h, for different CPM schemes (different L, M and $g(t)$) are given. From these plots, the best M, L, h and $g(t)$ that gives the highest distance; i.e., the lowest probability of error, can be chosen.

4.1.2 Properties of the CPM Schemes Selected for This Work

The two CPM schemes that we have selected for this thesis are:

- Scheme 1: Alphabet size, $M = 4$, Raised Cosine frequency pulse with length, $L = 3$, modulation index, $h = 0.3125$, and minimum squared Euclidean distance, $d_{\min}^2 = 1.480$;

- Scheme 2: Alphabet size, $M = 4$, Gaussian frequency pulse with $BT = 0.25$, pulse length, $L = 3$, modulation index, $h = 0.625$, and minimum squared Euclidean distance, $d_{\min}^2 = 4.693$.

The two CPM schemes we have chosen have different bandwidth efficiency and error performance. As discussed in [15, Chapter 5], $M = 4$ is a good alphabet size for obtaining a high d_B^2, and for this value of M, $L = 3$ is the optimum length of the frequency pulse. Therefore, for both of the schemes, we have chosen $M = 4$ and $L = 3$. Also, smaller values of h yield narrower bandwidth but poor error performance, while the opposite happens with higher value of h. From the plots in [15], it can be seen that for $M = 4$ and 3RC systems, a modulation index close to 0.6 has a very high d_B^2 and therefore very good error performance. For Scheme 1 we chose a smaller value of h (0.3125) and the RC pulse, to obtain a bandwidth efficient scheme. For Scheme 2 on the other hand we chose a higher value of h (0.625) and the Gaussian frequency pulse to obtain a higher minimum distance and therefore lower probability of error.

4.1.3 Discrete-Time Representation of CPM

For representing the CPM signal in discrete-time, we have followed the approach where the CPM modulator is implemented entirely in discrete time without considering the continuous-time version of the signal.

The samples per symbol time, N, is defined by

$$N \triangleq \frac{T}{T_s} \tag{4.19}$$

where T is the symbol interval, and T_s is the spacing between samples. The

current symbol index, n, is defined by

$$nN \leq l < (n+1)N \tag{4.20}$$

where l represents the sample index and is analogous to t in the continuous-time domain. The frequency signal is given by

$$\mathbf{f}[l; \boldsymbol{\beta}] = h \sum_{p=n-L+1}^{n} \beta[p]\mathbf{g}[l - pN] \tag{4.21}$$

where the symbols carry the same meaning as in (4.10). The vector, $\mathbf{g}[l - pN]$, has length N and contains the N discrete samples from the frequency response function, $g(t)$, corresponding to the p_{th} symbol interval. The phase of the signal, $\boldsymbol{\phi}[l; \boldsymbol{\beta}]$, is obtained by integrating the frequency signal in discrete-time. Following the *backward difference rule* for discrete-time integration [19] the phase, $\boldsymbol{\phi}[l; \boldsymbol{\beta}]$, can be expressed as

$$\boldsymbol{\phi}[l; \boldsymbol{\beta}] = \boldsymbol{\phi}[l - 1; \boldsymbol{\beta}] + \pi T_s \mathbf{f}[l - 1; \boldsymbol{\beta}]. \tag{4.22}$$

$\boldsymbol{\phi}[l; \boldsymbol{\beta}]$ can be separated into two terms, as was shown in Eq 4.11 for the continuous-time case

$$\boldsymbol{\phi}[l; \boldsymbol{\beta}] = 2\pi h \sum_{p=n-L+1}^{n} \beta[p]\mathbf{q}[l - pN] + \pi h \sum_{p=-L+1}^{n-L} \beta[p]$$

$$= \boldsymbol{\theta}[l; \boldsymbol{\beta}[n]] + \theta[n] \tag{4.23}$$

where the length N vector, $\boldsymbol{\theta}[l; \boldsymbol{\beta}[n]]$, is a function of the correlative state vector, $\boldsymbol{\beta}[n]$, and $\theta[n]$ is a scalar, representing the phase state, which can be computed the same way as in the continuous-time case. $\mathbf{q}[l - pN]$ is the length N vector

containing the discrete samples from the phase response function, $q(t)$.

Finally, the discrete-time CPM sequence is given by

$$\mathbf{s}[l; \boldsymbol{\beta}] \triangleq \exp\{j\boldsymbol{\phi}[l; \boldsymbol{\beta}]\}. \tag{4.24}$$

or in scalar form, each sample from the discrete-time CPM sequence is given by

$$s[l; \boldsymbol{\beta}] \triangleq \exp\{j\phi[l; \boldsymbol{\beta}]\}. \tag{4.25}$$

A detailed analysis on the discrete-time representation can also be found in [19].

In this thesis, for constructing the discrete-time representation of the CPM signal, we are going to consider very small values of N. As a result, the transmitting waveform will be an under-sampled discrete-time CPM signal. Our purpose is to investigate how well the conventional signal processing algorithm perform with a sampling rate below the Nyquist rate.

According to the Nyquist sampling theorem, for a band-limited signal with bandwidth B, the sampling rate has to be at least twice the bandwidth $(2B)$ for perfect reconstruction of the sampled waveform. However, since CPM signals are not band-limited [15] it is not possible to define a finite Nyquist sampling rate for CPM signals. As a result, depending on the parameters h, L, M and $q(t)$, some amount of frequency aliasing is always expected in the CPM signal spectrum, no matter what the sampling rate is. Hence, in this work, we are going to use the smallest possible sampling rate for the CPM waveform to demonstrate the performance of the proposed CPM-SC-FDMA scheme in LTE.

4.2 CPM-SC-FDMA Signal Generation

In our proposed scheme, the input data bits from each user are first CPM modulated, and then the samples from the CPM modulator are fed to the SC-FDMA system as input symbols. For subcarrier mapping the Interleaved subcarrier mapping method (IFDMA) is considered. The output of the SC-IFDMA system will be used to generate the continuous-time signal which will be transmitted.

Let us consider an SC-IFDMA system with a total of N_{total} subcarriers and J users, each of whom will be allocated K subcarriers for transmitting the data symbols. We assume that each user is transmitting P CPM symbols at a time, with each symbol carrying $m = log_2(M)$ bits, and the CPM waveform is sampled at a rate N samples per symbol time (T). So the effective number of information bits per sample will be m/N. Furthermore, for each user there will be PN number of samples coming out of the CPM modulator, and since each user is allocated K subcarriers, $K = PN$ and $N_{\text{total}} = JPN$. The PN CPM samples from the i_{th} user is denoted by the vector,

$$\mathbf{s}_i = [s_{i,0}, \ s_{i,1}, \ \ldots \ s_{i,PN-1}]. \tag{4.26}$$

Each element of $\mathbf{s}_i$ is given as

$$s_{i,l} = s[l; \beta] \tag{4.27}$$

which was defined in (4.25) as

$$s[l; \beta] \stackrel{\triangle}{=} \exp\left\{j\phi[l; \boldsymbol{\beta}]\right\}. \tag{4.28}$$

For each user, the block of data samples entering the DFT block is given

in Eq 4.26, and outputs of the $K(= PN)$ point DFT operation is given by the following equation

$$S_{i,k} = \sum_{l=0}^{PN-1} s_{i,l}\exp(-j2\pi kl/PN) \tag{4.29}$$

where $k = 0, \ \ldots \ , PN - 1$ denotes the discrete frequency index. Outputs of the DFT operation are mapped to a set of K subcarriers which are uniformly spaced across the whole bandwidth, and zeros are assigned to the remaining $N_{\text{total}} - K$ subcarriers. The subcarrier mapping can be expressed by the following equation

$$\text{Mapped symbols}, Y_{i,q} = \begin{cases} S_{i,k} & q = kJ + i \\ 0 & \text{otherwise} \end{cases} \tag{4.30}$$

where i denotes the user index ($i \in \{0, \ \ldots \ , J - 1\}$) and also the subcarrier number from which the subcarrier allocation starts. For example, the subcarrier allocation starts from $(0, \ 1, \ \ldots \ , J - 1)_{\text{th}}$ location, for $(0, \ 1, \ \ldots \ , J - 1)_{\text{th}}$ user respectively.

The mapped symbols are then transformed into the time domain by means of an $N_{\text{total}}(= JPN)$ point IDFT operation, expressed by the following equation

$$y_{i,l} = \frac{1}{JPN} \sum_{q=0}^{JPN-1} Y_{i,q}\exp(j2\pi ql/JPN) \tag{4.31}$$

where $l = 0, \ \ldots \ , JPN - 1$ represents the sample index. As discussed in Section 3.5, the output time samples from the IDFT operation can be shown to consist of the scaled and rotated version of the original input sequence $s_{i,l}$, which are repeated J times; i.e.,

$$y_{i,l} = \frac{1}{J}s_{(i,l)\bmod K} \cdot e^{j2\pi il/N_{\text{total}}}. \tag{4.32}$$

The phase rotation results from multiplication by the factor $e^{j2\pi il/N_{\text{total}}}$, and the J times repetition is expressed by the mod K notation. Also, as discussed in Section 3.5, the sample duration gets reduced by a factor of J. So, each sample $y_{i,l}$ now has a duration, $\tilde{T} = \frac{T}{J}$.

To prevent against interference in frequency selective multipath channel, Cyclic prefix is added to the time domain SC-FDMA samples by appending the last C_pN samples of the output sequence of the IDFT operation ($\mathbf{y}_i$) to the beginning of the data block, where it is assumed that the channel impulse response, denoted by $\mathbf{h}(t)$, has a duration less than C_pT seconds. So, the resultant sequence, $\tilde{\mathbf{y}}_i$, now has a length of $JPN + C_pN$.

The cyclic prefix serves two purposes: eliminates interblock interference by working as a guard band between blocks of data symbols since the first C_pN samples of the block, affected by interference from previous block, can be discarded without any loss of information and turns the linear convolution process between the sequence $\mathbf{y}_i$ and the channel impulse response, into a circular convolution process. As a result, the desired sequence can be extracted from the channel output by simple Frequency Domain Equalization (FDE) method, as discussed in the next section.

Next, the $JPN + C_pN$ samples are converted to a continuous-time waveform by pulse shaping using the pulse, $G(t)$, as shown in the following equation

$$\text{Continuous-time signal, } x_i(t) = \sum_{n=-C_pN}^{JPN-1} y_{i,l}G(t - \tilde{T}) \qquad (4.33)$$

In this thesis, we have used the Spectral Raised Cosine (SRC) pulse for pulse

shaping, defined by the following equation

$$G_{SRC}(t) = \frac{\sin(\pi t/\tilde{T})}{\pi t/\tilde{T}} \frac{\cos(\pi \alpha t/\tilde{T})}{1 - 4\alpha^2 t^2/\tilde{T}^2}. \tag{4.34}$$

Here, α represents the roll-off factor.

4.3 CPM-SC-FDMA Signal Reception

In uplink, the receiver, located at the base station, receives the combined signal from all the users. The received signal is first transformed into the frequency domain by a DFT operation, and then each user's data is extracted by a subcarrier de-mapping process. If the channel is frequency-selective then equalization is required to remove the effect of the channel. After the equalization process, the signal is transformed back into the time domain, and finally the symbols are detected using the Viterbi Algorithm (VA).

The continuous-time received signal $r(t)$ is sampled to generate the discrete-time sequence $\mathbf{r}$. The first $C_p N$ samples corresponding to the cyclic prefix are discarded, and the sequence consisting of the remaining JPN signal samples can be expressed by the following equation

$$\mathbf{r} = \sum_{i=0}^{J-1} \mathbf{h} \otimes \mathbf{y}_i + \mathbf{n} \tag{4.35}$$

where $\mathbf{y}_i$ is the sequence transmitted by the $i_t h$ user terminal, $\otimes$ denotes the circular convolution operation, and $\mathbf{h}$ is the discrete-time version of the channel impulse response $h(t)$. $\mathbf{n}$ represents the complex valued additive white Gaussian noise with zero mean and one sided PSD, N_0. For the AWGN channel, $\mathbf{h}$ is equal to 1; i.e., the transmitted sequence is affected by only the additive white

noise. The time-domain sequence, $\mathbf{r}$ is transformed into the frequency domain by a $N_{\text{total}} = JPN$ point DFT operation, as expressed in the following equation

$$\tilde{R}_k = \sum_{l=0}^{JPN-1} r_l \exp\left(-j2\pi kl/JPN\right) \tag{4.36}$$

where $k = 0, \ldots, JPN$ represents the discrete frequency index, and l represents the sample index in the time domain. The desired portion of the signal that is transmitted by the i_{th} user can be extracted by a subcarrier de-mapping process following the same algorithm by which subcarrier mapping was done in the transmitter. This is shown by the following equation

$$R_{i,q} = \tilde{R}_k \quad \text{for} \quad k = qJ + i \tag{4.37}$$

where $q = 0, \ldots, PN - 1$. $\mathbf{R}_i$ represents the frequency domain sequence corresponding to the i_{th} user's transmission and contains PN frequency domain samples.

If the signal is transmitted through a frequency selective channel then the next step is the FDE process , which is required in order to remove the effect of the channel. For the AWGN channel, however, this step is not needed. Assuming that the tapped delay profile of the channel impulse response, $\mathbf{h}$, is known to the receiver, the frequency domain coefficients of the channel associated with the i_{th} user's transmission can be obtained by a JPN point DFT operation, followed by a coefficient de-mapping process. This is shown in the following equations

$$\tilde{H}_k = \sum_{l=0}^{JPN-1} h_l \exp\left(-j2\pi kl/JPN\right) \tag{4.38}$$

$$H_{i,q} = \tilde{H}_k \quad \text{for} \quad k = qJ + i \tag{4.39}$$

where $q = 0, \ \ldots \ , PN - 1$.

The received signal can be expressed in the frequency domain as

$$R_{i,q} = H_{i,q}S_{i,q} + W_q \tag{4.40}$$

where W_q is the DFT of the noise sequence **n**.

The equalized sequence, $\hat{R}_{i,q}$ is obtained by multiplying $R_{i,q}$ by the equalizer coefficients

$$\hat{R}_{i,q} = \hat{H}_{i,q}R_{i,q}. \tag{4.41}$$

where in case of the Zero Forcing (ZF) equalizer $\hat{H}_{i,q}$ is expressed as

$$\hat{H}_{i,q} = \frac{1}{H_{i,q}} \tag{4.42}$$

and if the MMSE (Minimum Mean Square Error) equalizer is used then $\hat{H}_{i,q}$ is expressed as

$$\hat{H}_{i,q} = \frac{H_{i,q}^*}{|H_{i,q}|^2 + 1/\left(E_s/N_0\right)}. \tag{4.43}$$

E_s/N_0 represents the sample energy-to-noise ratio. The equalized sequence, $\hat{R}_{i,q}$ is obtained by multiplying $R_{i,q}$ by the equalizer coefficients

$$\hat{R}_{i,q} = \hat{H}_{i,q}R_{i,q}. \tag{4.44}$$

Next, the frequency domain samples are transformed back into time domain

by a PN point IDFT operation.

$$\hat{r}_{i,l} = \frac{1}{PN} \sum_{q=0}^{PN-1} \hat{R}_{i,q} \exp(j2\pi ql/PN). \tag{4.45}$$

4.4 Symbol Detection Using the Viterbi Algorithm

The optimum receiver for CPM is based on the Maximum Likelihood Sequence Detection (MLSD) principle, which selects the most likely sequence corresponding to the received signal by conducting a search through the trellis for the path with the minimum Euclidean distance. The Viterbi Algorithm (VA) is an efficient method for performing this search. In this section we provide a brief discussion on applying the VA for detecting the CPM modulated SC-IFDMA symbols. A detailed analysis on application of the VA for CPM can be found in [15].

The decision rule for MLSD is based on minimizing the Euclidean Distance between the received signal and all possible transmitted signals. For continuous time, the decision rule can be shown to be equivalent to

$$\hat{\boldsymbol{\beta}} = \arg \max_{\tilde{\boldsymbol{\beta}}} \operatorname{Re} \left\{ \int_{-\infty}^{\infty} r(t)s^*(t;\tilde{\boldsymbol{\beta}})dt \right\} \tag{4.46}$$

i.e., the maximum likelihood sequence, $\hat{\boldsymbol{\beta}}$, is the one that maximizes the correlation of the received signal with the hypothetical transmitted signal, $s^*(t;\tilde{\boldsymbol{\beta}})$. In practice, for calculating the correlation output, a recursive method is followed, as described in [15], by defining

$$J_n(\hat{\boldsymbol{\beta}}) \triangleq \operatorname{Re} \left\{ \int_{-\infty}^{(n+1)T} r(t)s^*(t,\tilde{\boldsymbol{\beta}})dt \right\}$$

$$= J_{n-1}(\tilde{\boldsymbol{\beta}}) + Z_n(\tilde{\boldsymbol{\beta}}) \tag{4.47}$$

where n represents the symbol index and

$$Z_n(\tilde{\boldsymbol{\beta}}) \triangleq \mathrm{Re} \left\{ \int_{nT}^{(n+1)T} r(t) s^*(t; \tilde{\boldsymbol{\beta}}) dt \right\} \tag{4.48}$$

Applying (4.1) we get

$$Z_n(\tilde{\boldsymbol{\beta}}) = \mathrm{Re} \left\{ \int_{nT}^{(n+1)T} r(t) e^{-j\phi(t; \tilde{\boldsymbol{\beta}})} dt \right\}$$

$$= \mathrm{Re} \left\{ e^{-j\theta_n} \int_{nT}^{(n+1)T} r(t) e^{-j\theta(t; \tilde{\boldsymbol{\beta}})} dt \right\} \quad \text{[from (4.11)]}. \tag{4.49}$$

In other words, the correlation output for the n_{th} symbol interval can be calculated by adding the metric, $Z_n(\tilde{\boldsymbol{\beta}})$ to the correlation metric for the previous symbol interval. At each symbol interval, for a particular state, σ, the algorithm calculates the correlation metric for all the branches of the trellis that ends at σ and selects the branch with the highest metric as the survivor while discarding all the others. This is done for all the states in the trellis. This process is repeated at each new symbol arrival and is continued until the final symbol is received. At the final step, the state with the highest metric is selected as the "global survivor". Then, the algorithm "traces back" along the path of the survivor branches, starting from global survivor state.

In the CPM-SC-IFDMA receiver, the outputs of IDFT operation can be viewed as noisy, discrete-time samples from a continuous-time CPM waveform. The VA is applied in discrete-time following the same principle as in continuous time. The

discrete-time equivalent of (4.48) can be written as

$$Z_n[\tilde{\boldsymbol{\beta}}] = \text{Re} \left\{ \sum_{p=l}^{p=l+N} r_{i,p} s^*[l; \boldsymbol{\beta}] \right\} \tag{4.50}$$

where $r_{i,p}$ is the p_{th} sample from the i_{th} user's transmission, and l represents the current sample index. (4.50) can also be written in matrix form

$$Z_n[\tilde{\boldsymbol{\beta}}] = \text{Re} \left\{ \mathbf{r}_i^T \mathbf{s}^*[l; \boldsymbol{\beta}] \right\} \tag{4.51}$$

$$= \text{Re} \left\{ e^{-j\theta[n]} \, \mathbf{r}_i^T \, e^{-j\boldsymbol{\theta}[l;\tilde{\boldsymbol{\beta}}]} \right\} \tag{4.52}$$

where $\mathbf{s}^*[l; \boldsymbol{\beta}]$ and $e^{-j\boldsymbol{\theta}[l;\tilde{\boldsymbol{\beta}}]}$ are assumed to be $N \times 1$ vectors; $\mathbf{r}_i$ is also an $N \times 1$ vector which contains the N samples from the i_{th} user's transmission, corresponding to the current symbol interval, and $()^T$ represents a matrix transpose operation. Thus the CPM-SC-IFDMA samples are detected using the Viterbi algorithm.

Chapter 5

Application of CPM-SC-IFDMA in LTE

The goal of this work is to develop a transmission scheme for uplink LTE which has better performance with respect to power and spectral efficiency than the current technology being considered for LTE. To achieve this goal we have selected CPM as the modulation scheme which is one of the most power and spectral efficient phase modulation technique, and combined it with the multiple access scheme–IFDMA, which has the lowest PAPR of the two SC-FDMA schemes (IFDMA and LFDMA). In this chapter, we discuss the advantages of the proposed scheme over the current technology specified in LTE.

5.1 Effect of High PAPR

High PAPR is one of the most challenging implementation issues that the designers of a transmission scheme have to deal with. It degrades the performance of the RF power amplifier and other non-linear devices like the DAC (Digital to

Analog Converter) in the transmitter and the ADC (Analog to Digital Converter) in the receiver. The RF power amplifier is the most expensive component in a transmission chain. In order to avoid distortion, it needs to be operated in the linear region. Therefore the peak value of the input must be constrained to be in this region (less than or equal to the saturation level). This is done by decreasing the average power of the input signal, referred to as input power back-off, which is approximately equal to the PAPR (depending on the specifics of the amplifier). So if the peak power of the input is too high compared to the average i.e.; high PAPR, then on average, the power amplifier is underutilized by a back-off amount. Thus high PAPR requires high input power back-off which reduces the power efficiency of the RF amplifier and may limit the battery life for mobile applications. In addition to that, the coverage range of the mobile device is reduced, and the cost is higher than what would be needed by the average power requirements. Furthermore, a high PAPR requires high resolution for both the transmitter's DAC and the receiver's ADC, as the dynamic range of the signal is proportional to the PAPR which places an additional complexity, cost, and power burden on the system [1, Chapter 4]. Therefore, reducing the PAPR is the primary target when designing a power efficient scheme.

5.2 Advantage of CPM-SC-IFDMA

The modulation schemes currently specified for uplink LTE are: QPSK, 16QAM and 64QAM [12]. In QAM modulation schemes, two carriers shifted in phase by 90 degrees are modulated, and the resultant output consists of both amplitude and phase variations. QAM schemes require linear amplifiers because of the amplitude variation which makes them power inefficient. QPSK can be considered as

a special case of QAM where only the phase of the carrier signal is varied and the amplitude stays constant. QPSK is a constant envelope modulation method but the phase variation in a QPSK waveform can be as large as $\pm\pi$ which may make the envelope go to zero momentarily. This causes large envelope fluctuation in QPSK waveforms which results in high PAPR. The phase discontinuity in QPSK waveforms also causes them to occupy larger bandwidths and results in bandwidth inefficiency.

CPM schemes on the other hand, because of the continuous phase and constant envelope property, are known to be both power and bandwidth efficient. The benefit of combining IFDMA with CPM is that the constant envelope property of CPM can be maintained in the resultant transmitted signal. As we have shown in Section 3.5, in IFDMA, the transmitted signal consists of a scaled and rotated version of the actual input symbols. So, the amplitude of the transmitted signal is determined by the amplitude of the input symbols. In the proposed scheme, the constant amplitude CPM samples are the input symbols to the SC-IFDMA system. Therefore, combining IFDMA with CPM generates a constant-amplitude transmitted signal with a very low PAPR. The PAPR of a continuous-time signal was defined in (3.3), in Section 3.6. For a discrete-time CPM-SC-IFDMA signal, sampled at N samples per symbol time and without pulse shaping, the PAPR is 0 dB; i.e.,

$$\text{PAPR} = 10\log_{10}\left(\frac{\max\limits_{0\leq l\leq PN-1}|s_{i,l}|^2}{\frac{1}{PN}\sum_{l=0}^{PN-1}|s_{i,l}|^2}\right) = 0 \text{ dB} \tag{5.1}$$

where $s_{i,l}$ represents the constant amplitude samples from the i_{th} user's transmitted signal and was defined in (4.25). The PAPR is 0 dB also for NRZ (non-return-to-zero) pulse shaping and MPSK modulated SC-FDMA. With non-NRZ pulse shaping, the PAPR is much higher compared to that with NRZ pulse shaping.

LTE has selected LFDMA as the multiple access scheme for uplink. But the transmitted signal in LFDMA consists of weighted sums of all the input symbols in the block in addition to the actual input symbols, as shown in Section 3.5. Because of this, the amplitude of the time domain signal is not constant, no matter what the input symbol amplitude is. So, it is not possible to preserve the constant amplitude property of CPM if it is combined with LFDMA, instead of IFDMA.

The PAPR of a signal can be characterized by its numerically calculated CDF (Cumulative Distribution Function). CDF represents the probability that PAPR is less than a certain PAPR which is plotted along the x-axis and the corresponding CDF is plotted along the y-axis to graphically represent the PAPR of a signal. The PAPR plots of QPSK and 16-QAM modulated SC-FDMA, with different subcarrier mapping, given in [3, Fig. 7.5], show that IFDMA schemes have much lower PAPR than LFDMA schemes (for both QPSK and 16-QAM). The PAPR plots in [3] also show that when pulse shaped with the SRC pulse, the impact of the roll-off factor, α on the PAPR, is more obvious in the case of IFDMA, where the PAPR increases significantly as α decreases from 1 to 0. Increasing α increases the out-of-band radiation; so for QPSK and 16-QAM modulated IFDMA, there is a trade-off between the power and bandwidth efficiency.

We have shown a comparison between the PAPR of CPM (Scheme 1) modulated SC-IFDMA and SC-LFDMA in Fig. 5.1. The PAPR is calculated assuming a total of 300 subcarriers, shared by 2 users in a 5 MHz transmission channel. The SRC pulse was truncated to ± 10 symbol intervals and the transmitted signal was oversampled by a factor of 10. Fig. 5.1 shows that at high percentiles (approximately 90%) of the CDFs, the PAPR of the IFDMA scheme is approximately 7.5

dB lower than that of LFDMA for roll-off factor, $\alpha = 1$. The difference in PAPR decreases as α decreases, but even at $\alpha = 0$, IFDMA has a lower PAPR than LFDMA by aprroximately 5 dB. Also note that, with CPM modulated IFDMA, the increase in PAPR with the decrease of α is much lower than that of QPSK and 16-QAM modulated IFDMA, shown in [3]. So, the trade-off between power and bandwidth efficiency is not so significant in case of CPM modulated SC-IFDMA as in QPSK or 16-QAM modulated SC-IFDMA.
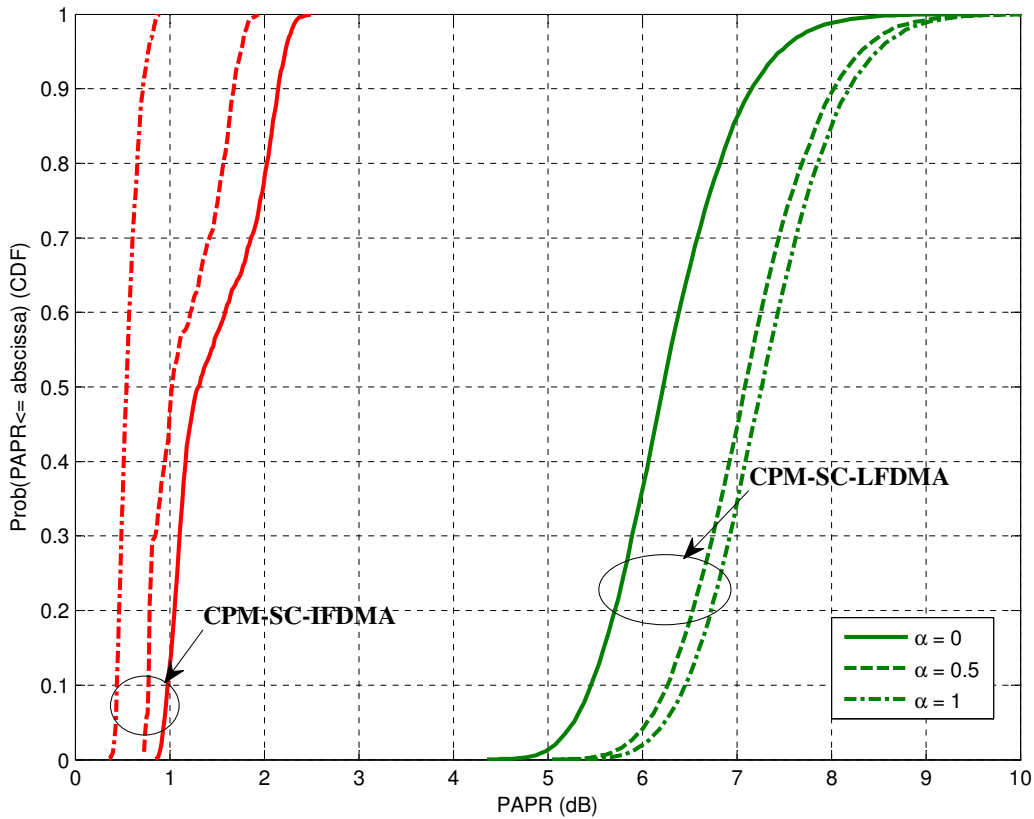

Figure 5.1. PAPR of CPM-SC-IFDMA and CPM-SC-LFDMA. The solid lines, dashed lines and dashed-dotted lines show the results for $\alpha = 0, \alpha = 0.5$, and $\alpha = 1$ respectively.

5.3 Insertion of Guard Band

In LTE, IDFT size for a particular bandwidth, $N_{\text{IDFT/DFT}}$, is specified to be larger than the number of usable subcarriers, N_{total}, and equal to the next power of 2, in order to constitute the guard band in the frequency domain, and also to increase the computational efficiency of the IDFT (Tx)/DFT (Rx) operation, as discussed in Section 2.3. The guard band is thus implemented by assigning zeros to the unused subcarrier during the IDFT operation in the transmitter. But the time domain representation of IFDMA and LFDMA schemes, given in (3.1) and (3.2) respectively, in Section 3.5, were derived (detailed derivation can be found in [3] and also provided in Appendix A) assuming the IDFT size to be equal to the number of occupied subcarriers. The low PAPR feature of IFDMA comes from its unique property of having the resultant time domain signal containing the actual input symbols only, which is lost if N_{total} is not equal to $N_{\text{IDFT/DFT}}$. The impact of $N_{\text{IDFT/DFT}}$ not being equal to N_{total} on the PAPR is shown in Fig. 5.2, where the PAPR of a CPM modulated IFDMA waveform is shown for the two cases: $N_{\text{IDFT/DFT}} = N_{\text{total}}$ and $N_{\text{IDFT/DFT}} > N_{\text{total}}$. The simulation is done assuming 2 users and for the 5 MHz channel, where the number of usable subcarriers (N_{total}) and the IDFT size ($N_{\text{IDFT/DFT}}$) are specified in LTE to be 300 and 512 respectively. The CPM scheme chosen here is Scheme 1 and value of the roll-off factor for the SRC pulse is 0.
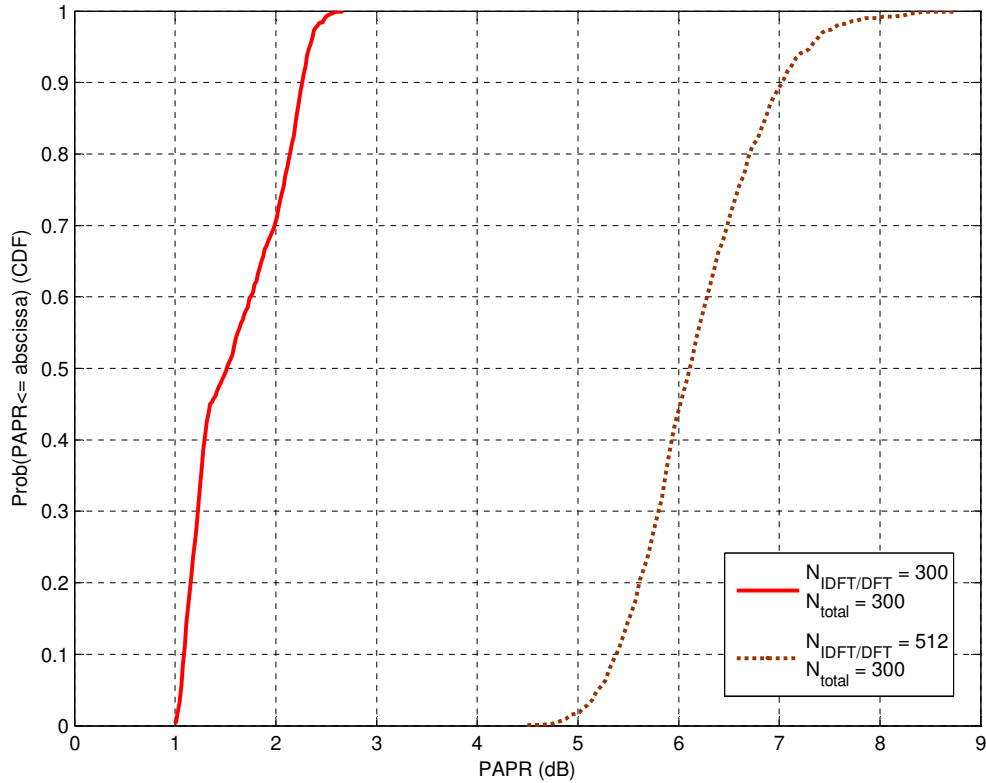
Figure 5.2. Effect of guard band on the PAPR of a CPM-SC-IFDMA waveform.

As can be seen in Fig. 5.2, the PAPR of the CPM-SC-IFDMA increases by approximately 5 dB (at 90% CDF) when $N_{\text{IDFT/DFT}}$ is greater than N_{total}. Therefore, in order to maintain the power efficiency of the proposed scheme, we will not implement the guard band as zeros in the IDFT, and take the IDFT size equal to the number of occupied subcarriers. The insertion of a frequency guard band can be achieved by simply moving the center of the used band to the desired distance (in frequency) away from the next occupied channel. Since the specified N_{total} is not a power of 2, some amount of computational efficiency will be lost, which is not significant compared to the benefits achieved.

5.4 Maximal Ratio Combining

In LTE, a two-antenna based receiver structure is used, and Maximal Ratio combining (MRC) is applied to combine the two received signals. MRC is a well-known diversity-combining technique where signals from several antenna elements are weighted and combined to maximize the output signal-to-interference-plus-noise ratio (SINR). In our work we have applied MRC for signals received in the frequency selective multi-path channels. The signal combining is done in the frequency domain, on a subcarrier-by-subcarrier basis. The equation for received signal in frequency selective multi-path channels is given in (4.40). As we have discussed in Section 4.3, in order to compensate for the channel effect; i.e., to remove the effect of multiplication by $\mathbf{H}_i$ (the frequency domain coefficients of the channel associated with the i_{th} user's transmission), frequency domain equalization is applied. But for this work, we apply MRC, followed by an amplitude scaling, the combined effect of which compensates for the channel effect and therefore, equalization is not required. The transmitter and receiver configuration and the frequency domain coefficient vector corresponding to the two receiving antennas, $\mathbf{H}_{i,1}$ and $\mathbf{H}_{i,2}$, are shown in Fig. 5.3.
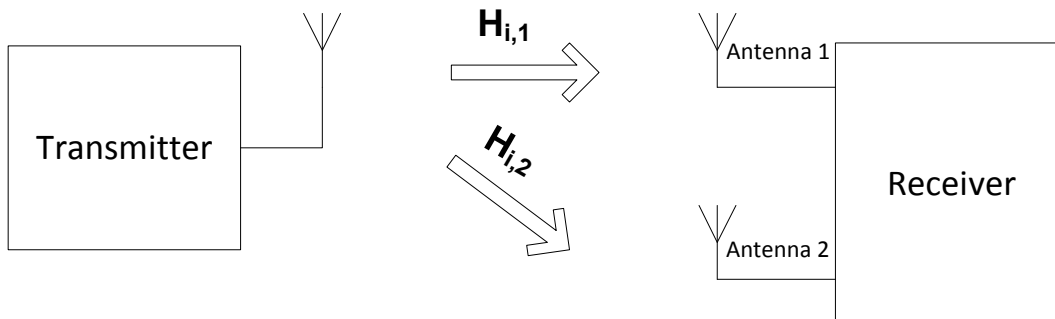

Figure 5.3. Transmitter and receiver configuration for MRC.

To apply MRC, first the signals received via the two antennas are each multiplied in frequency domain with the complex conjugated version of $\mathbf{H}_{i,1}$ and $\mathbf{H}_{i,2}$, and then they are summed. This process corrects the channel phase and blends the two received signals in the correct ratio. Then the combined signal is amplitude scaled by dividing by the factor $|\mathbf{H}_{i,1}|^2 + |\mathbf{H}_{i,2}|^2$. The amplitude scaling step makes sure that the received sequence has a similar amplitude as the transmitted sequence. These two steps together removes the channel effect and replaces the equalizer. The MRC and the amplitude scaling processes are shown by the following equation

$$\text{Combined Signal, } \hat{\mathbf{R}}_i = \frac{\mathbf{R}_{i,1}\mathbf{H}_{i,1}^* + \mathbf{R}_{i,2}\mathbf{H}_{i,2}^*}{|\mathbf{H}_{i,1}|^2 + |\mathbf{H}_{i,2}|^2} \tag{5.2}$$

where $\mathbf{R}_{i,1}$ and $\mathbf{R}_{i,2}$ are the frequency domain representations of the received signals via the two antennas.

Chapter 6

Simulation Results

In this chapter we discuss the BER (bit error rate) performance of the proposed scheme in the AWGN and three frequency selective channels, and compare with that of a convolutionally coded QPSK modulated SC-LFDMA (CC-QPSK-LFDMA) scheme. The delay profiles of the frequency selective channels have been taken from the 3GPP LTE specifications [6], and the simulation parameters are selected corresponding to the 5 MHz transmission channel parameters specified in LTE. The CPM schemes selected for the simulation are Scheme 1 and Scheme 2, whose properties were described in Section 4.1.1.

6.1 Selection of SC-FDMA Schemes for Comparison

The methodology for selecting the SC-FDMA schemes for comparison have been discussed in [4, Section VII]. As mentioned in [4], no studies have been conducted to obtain the numerically optimal CPM-SC-IFDMA schemes (Scheme 1 and Scheme 2), and the main reason for selecting these particular schemes was to select at least one CPM-SC-IFDMA scheme that possessed comparable bandwidth

and complexity to a CC-QPSK-based scheme. The convolutional code used for the CC-QPSK scheme is a rate $1/2$ code with a constraint length of 5 and octal generator polynomial [23, 35]. So, the CC-QPSK scheme has 4 bits in the memory and an information rate of 1 bit/symbol. This is also true for the CPM-SC-IFDMA schemes since both of them have alphabet size, $M = 4$, frequency pulse with length, $L = 3$ and are sampled at a rate, $N = 2$ samples per symbol. Thus, all three SC-FDMA schemes have similar complexities and information rate.

Our purpose is to demonstrate the BER performance of the proposed scheme in LTE specified channels and show comparison with that of a transmission scheme which LTE currently specifies. Since QPSK is one of the modulation methods that LTE uses and SC-LFDMA is chosen as the multiple access scheme for uplink LTE, we want to compare the performance of the CPM-SC-IFDMA scheme with that of a QPSK-LFDMA based scheme. Furthermore, combining the QPSK-LFDMA scheme with a convolutional encoding process introduces memory which makes it more comparable to CPM-SC-IFDMA as CPM is a memory based modulation method. The properties of the convolutional code that will be used in our work, are also the same as in [4], although the convolutional code specified in LTE has different properties (Section 2.3.3). Therefore, as explained above, the CC-QPSK-LFDMA scheme has similar complexities and information rate as the CPM-SC-IFDMA schemes.

6.2 PAPR properties

The PAPR plots of the SC-FDMA schemes are shown in Fig 6.1. The signals are pulse shaped using the SRC pulse, and the PAPRs are plotted for 3 different values of the roll-off factor ($\alpha = 0$, 0.5, and 1). The simulation is done assuming

a total of 300 subcarriers and 2 users, each occupying 150 subcarriers.
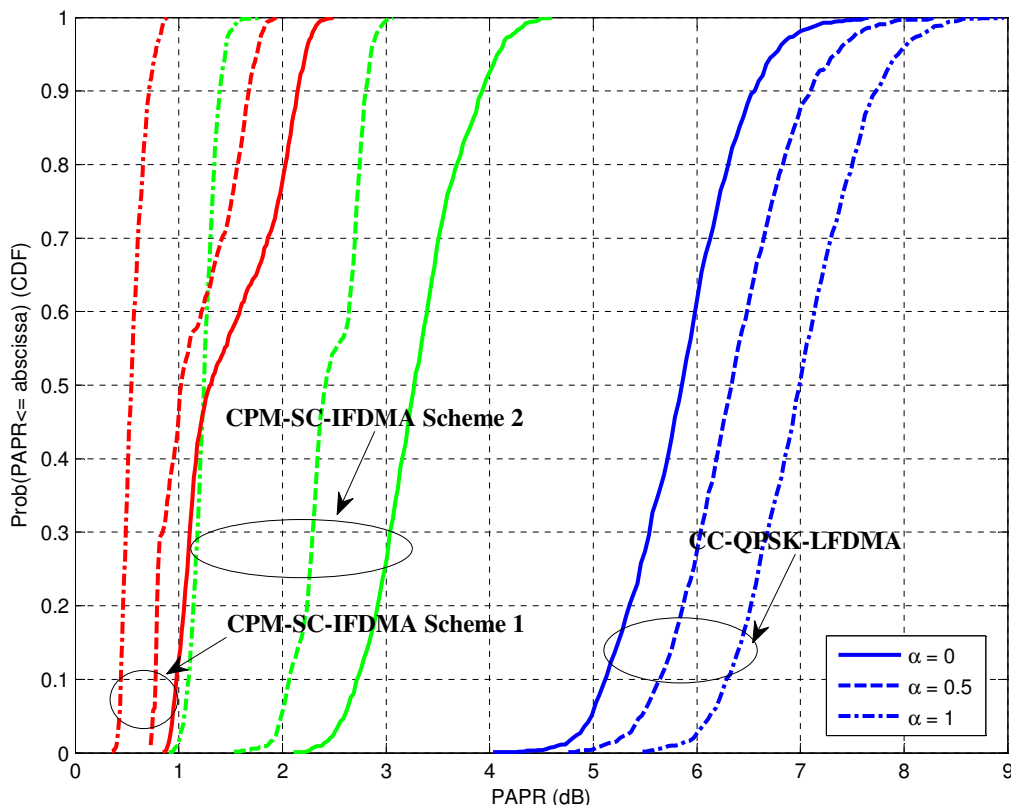
Figure 6.1. PAPR plots of CPM-SC-IFDMA Scheme 1, Scheme 2 and CC-QPSK-LFDMA assuming $J = 2$ users, $K = 150$ subcarriers per user and total subcarriers, $N_{\text{total}} = 300$ subcarriers. The solid lines, dashed lines and dashed-dotted lines show the results for $\alpha = 0$, $\alpha = 0.5$, and $\alpha = 1$ respectively.

As seen, the PAPR of both the CPM-SC-IFDMA schemes are much lower than the CC-QPSK-LFDMA scheme. Scheme 1 has lower PAPR than the other two schemes. Considering the 90% PAPR values we see that, for $\alpha = 0$, Scheme 1 has a 4.42 dB advantage over CC-QPSK-LFDMA while Scheme 2 has a 2.64 dB advantage over CC-QPSK-LFDMA. The PAPR difference between the CC-QPSK-LFDMA scheme and the CPM-SC-IFDMA schemes increases with the increase of α. The maximum PAPR advantage is 7 dB for Scheme 1 and 6.34 dB for

Scheme 2 (at 90% PAPR).

As we have discussed in Section 5.1, the PAPR value of a transmission scheme is a measure of how much input power back-off is required; in other words the PAPR indicates how much power efficiency is lost. Therefore, in order to make a true comparison between the BER performance of the CPM-SC-IFDMA schemes and the CC-QPSK-LFDMA scheme, the PAPR values are required to be added to the signal-to-noise-ratio (E_b/N_0) values, plotted along the X-axis in the BER plots. However, note that the input back-off values do not always have to be equal to the PAPR. It depends on the design of the power amplifier; the loss in the RF power can be made less than predicted by the PAPR values if special techniques are applied. In that case, our analysis should be regarded as upper limits of the performance difference between CPM-SC-IFDMA and CC-QPSK-LFDMA.

Table 6.1 shows the PAPR values at 90% and 99%, referred to as the IB$_{90\%}$ and IB$_{99\%}$ values respectively, for the three SC-FDMA schemes corresponding to three different values of the roll-off factor, α. To select which PAPR values are to be added, we compare the bandwidths of the CPM-SC-IFDMA schemes with that of the CC-QPSK-LFDMA scheme, corresponding to different values of the roll-off factor.

The PSDs of the three SC-FDMA schemes are plotted in Fig. 6.2. The simulation parameters are same as the PAPR plots. Assuming that the channel bandwidth is defined at a sidelobe decay level of -40 dB, observing Fig. 6.2, we see that Scheme 1 with $\alpha = 0.5$ and Scheme 2 with $\alpha = 0$ have similar bandwidth as CC-QPSK-LFDMA with $\alpha = 0$. The selected IB$_{90\%}$ and IB$_{90\%}$ values are highlighted in bold in Table 6.1.
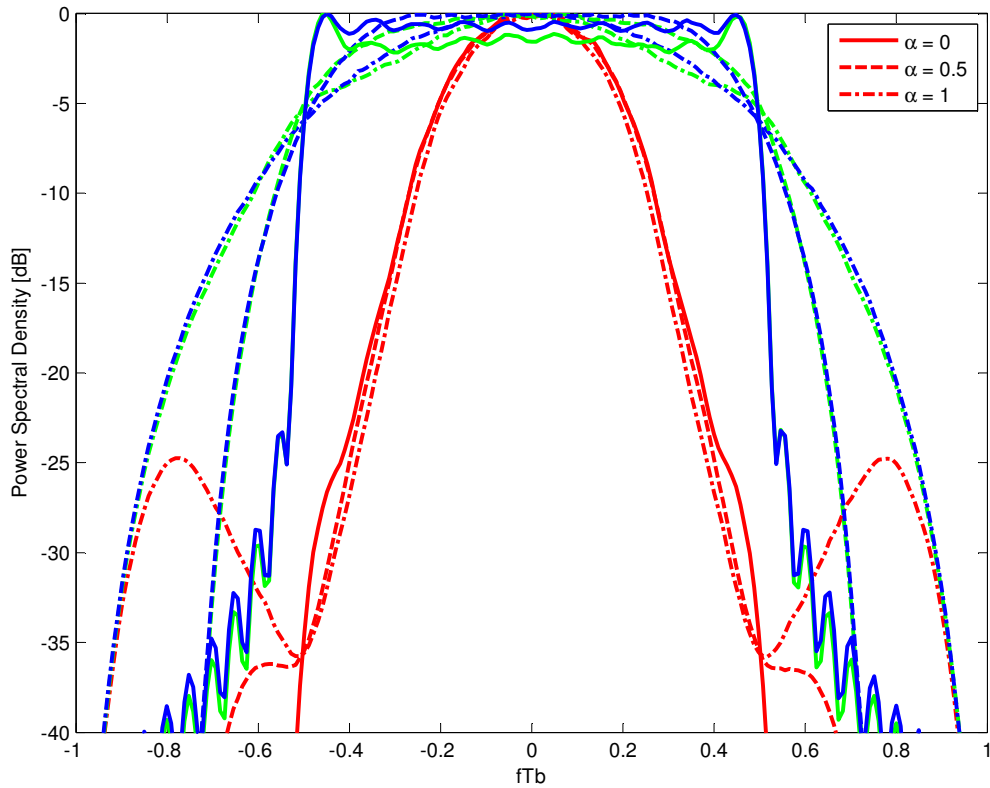
Figure 6.2. Power Spectral Density of CPM-SC-IFDMA Scheme 1, Scheme 2 and CC-QPSK-LFDMA assuming $J = 2$ users, $K = 150$ subcarriers per user and total subcarriers, $N_{\text{total}} = 300$ subcarriers. The color coding is as follows: red (medium dark in gray scale) represents Scheme 1, blue (dark in gray scale) represents Scheme 2, and green (light gray in gray scale) represents CC-QPSK-LFDMA. Solid lines, dashed lines and dashed-dotted lines show the results for $\alpha = 0$, $\alpha = 0.5$, and $\alpha = 1$ respectively.

6.3 BER Performance

The parameters selected for simulating the BER plots were taken from the 3GPP LTE specifications. The simulation parameters are listed in Table 6.2. All the simulations are done assuming 2 users, each of whom is allocated 150 subcarriers.

Scheme	IB$_{90\%}$ [dB]	IB$_{99\%}$	α
CPM-SC-FDMA Scheme 1	2.14	2.34	0
	1.67	**1.84**	**0.5**
	0.72	0.85	1
CPM-SC-FDMA Scheme 2	**3.92**	**4.35**	**0**
	2.81	2.96	0.5
	1.39	1.53	1
CC-QPSK-LFDMA	**6.56**	**7.22**	**0**
	7.12	7.83	0.5
	7.73	8.36	1

Table 6.1. Required Input Back-off Values from the PAPR Plots

Channel Bandwidth	5 MHz
Number of occupied subcarriers (N_{total})	300
IDFT/DFT size ($N_{\text{IDFT/DFT}}$)	300
Sampling rate (f_s)	7.68 MHz
Sample duration (T_s)	130 ns
CP duration	4.69μs (36 samples)

Table 6.2. Simulation Parameters.

We have chosen three frequency selective channels: the Extended Pedestrian A channel (EPA), the Extended Vehicular A channel (EVA), and the Extended Typical Urban channel (ETU), for analyzing the BER performance of the SC-FDMA schemes. In Table 6.3 the channel model parameters of the EPA, EVA and ETU channels are defined. In Table 6.4, 6.5 and 6.6 respectively, the tapped delay line models of the EPA, EVA and ETU channels are described. The values in Table 6.3–6.6 are taken from the technical specification of 3GPP LTE [6].

Model	Number of channel taps	Delay spread (r.m.s)	Maximum excess tap delay (span)
Extended Pedestrain A (EPA)	7	45 ns	410 ns
Extended Vehicular A (EVA)	9	357 ns	2510 ns
Extended Tyical Urban (ETU)	9	991 ns	5000 ns

Table 6.3. Delay profiles of the LTE channel models.

Not all the channel tap delays are integer multiples of the chosen sample du-

Excess tap delay [ns]	Relative power [dB]
0	0.0
30	-1.0
70	-2.0
90	-3.0
110	-8.0
190	-17.2
410	-20.8

Table 6.4. Extended Pedestrian A channel (EPA).

Excess tap delay [ns]	Relative power [dB]
0	0.0
30	-1.5
150	-1.4
310	-3.6
370	-0.6
710	-9.1
1090	-7.0
1730	-12.0
2510	-16.9

Table 6.5. Extended Vehicular A channel (EVA).

Excess tap delay [ns]	Relative power [dB]
0	-1.0
50	-1.0
120	-1.0
200	0
230	0
500	0
1600	-3.0
2300	-5.0
5000	-7.0

Table 6.6. Extended Typical Urban channel (ETU).

ration, T_s (= 130 ns); therefore, we first choose a different sample duration, T_{new}, which is computationally convenient, i.e.; a submultiple of the channel tap delays. The channel model is first obtained with this new sample duration and then down-sampled or up-sampled in order to obtain the actual channel model. For

this work, we have chosen $T_{\mathrm{new}} = 10$ ns, which is 13 times smaller than the actual sample duration (130 ns); therefore the channel model that is obtained by expressing the tap delays in multiples of $T_{\mathrm{new}} = 10$ ns, needs to be down-sampled by 13 times, to get the actual channel model. For example, for the EPA channel, the channel model based on a 10 ns sample duration is given in Table 6.7. A

Excess tap delay in terms of $T_{\mathrm{new}} = 10$ ns	Relative power [dB]
0	0.0
3	-1.0
7	-2.0
9	-3.0
11	-8.0
19	-17.2
41	-20.8

Table 6.7. EPA channel model based on 10 ns sample duration.

10 ns sample duration results in a sampling rate of 100 MHz, which is 13 times higher than the specified sampling rate for the 5 MHz transmission channel. So, we down-sample the model in Table 6.7 by 13 times.

Fig. 6.3 shows the BER plots of CPM-SC-IFDMA Scheme 1, Scheme 2 and CC-QPSK-LFDMA in the AWGN channel. Also the BER plots after compensating for the loss in power efficiency, i.e., adding the required input back-off values from Table 6.1, are plotted. For this work, we will show the results using the $\mathrm{IB}_{99\%}$ values only . The data points corresponding to the actual BER performance and the BER performance plotted as a function of $E_b/N_0 + \mathrm{IB}_{99\%}$ are shown with open markers and closed markers respectively. For comparing the BER performance of the three schemes, we have determined the E_b/N_0 required to achieve a BER of 10^{-5}.
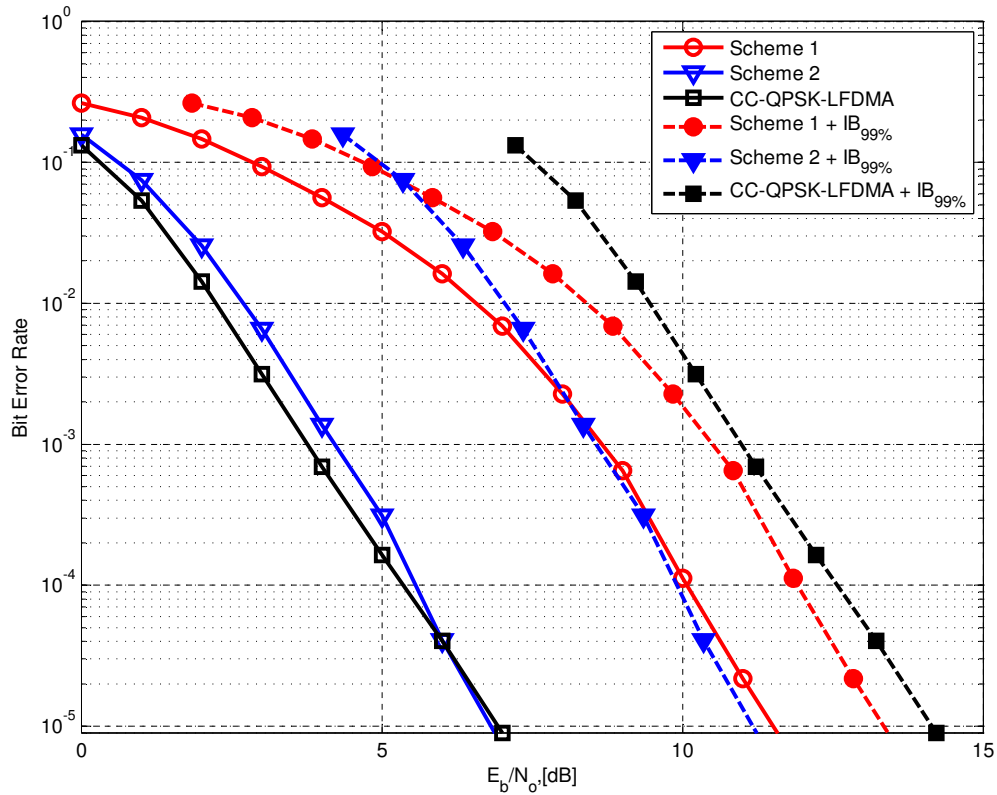
Figure 6.3. BER plots of CPM-SC-IFDMA Scheme 1, Scheme 2 and CC-QPSK-LFDMA in the AWGN channel, assuming $J = 2$ users, $K = 150$ subcarriers per user and total subcarriers, $N_{\text{total}} = 300$ subcarriers. Open markers show the BER performance vs E_b/N_0. The filled-in markers show the BER performance vs $E_b/N_0 + \text{IB}_{99\%}$ using the $\text{IB}_{99\%}$ values from Table 6.1.

As seen in Fig. 6.3, Scheme 2 and the CC-QPSK-LFDMA scheme achieves the target BER at $E_b/N_0 = 7$ dB, whereas Scheme 1 requires an $E_b/N_0 = 11.5$ dB. But when the BER results obtained after adding the $\text{IB}_{99\%}$ values are compared, we see that both Scheme 1 and Scheme 2 outperform the CC-QPSK-LFDMA scheme. As observed, Scheme 1 achieves the target BER at $E_b/N_0 = 13.4$ dB and Scheme 2 at $E_b/N_0 = 11.2$ dB, whereas the CC-QPSK-LFDMA scheme requires an E_b/N_0 of 0.8 dB and 3 dB higher than Scheme 1 and Scheme 2 respectively.

Fig. 6.4 shows the BER performance of the SC-FDMA schemes in the fre-

quency selective EPA channel. The figure shows the BER plots with and without compensating for the power efficiency loss; i.e., BER as a function of E_b/N_0 and also as a function of $E_b/N_0 + \text{IB}_{99\%}$.
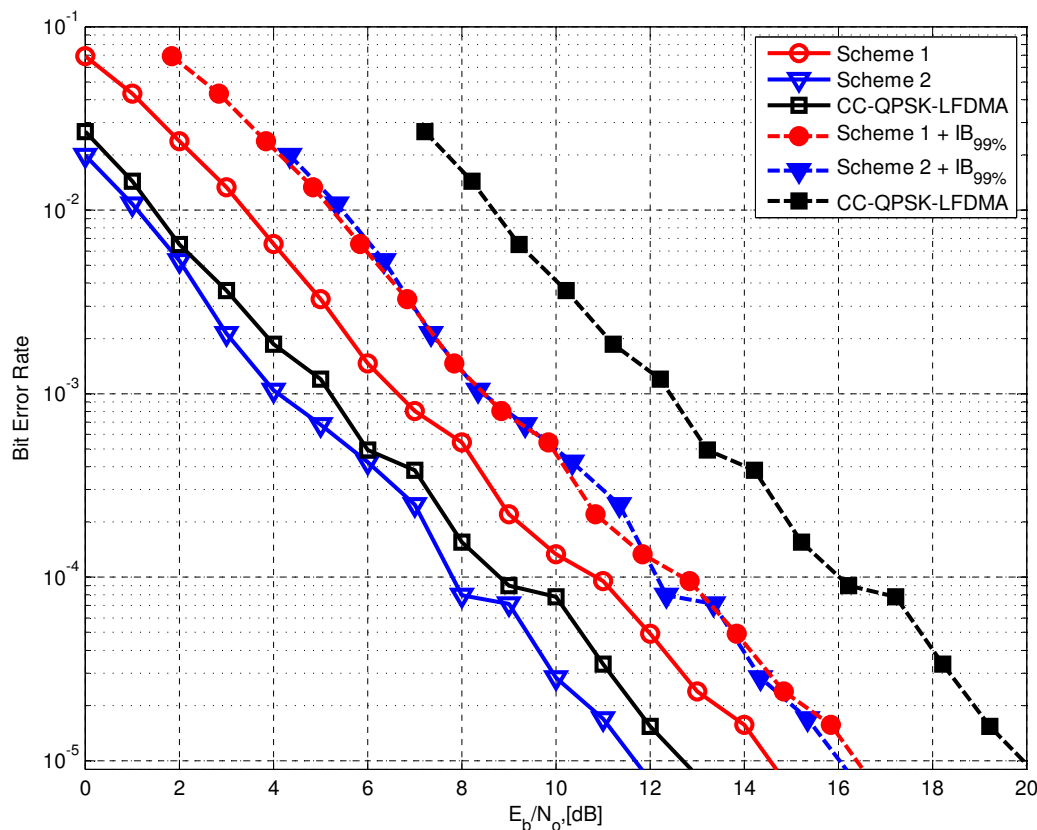

Figure 6.4. BER plots of CPM-SC-IFDMA Scheme 1, Scheme 2 and CC-QPSK-LFDMA in the EPA channel, assuming $J = 2$ users, $K = 150$ subcarriers per user and total subcarriers, $N_{\text{total}} = 300$ subcarriers. Open markers show the BER performance vs E_b/N_0. The filled-in markers show the BER performance vs $E_b/N_0 + \text{IB}_{99\%}$ using the $\text{IB}_{99\%}$ values from Table 6.1.

As can be observed, without taking the power efficiency into account, CC-QPSK-LFDMA has approximately 2 dB advantage over Scheme 1 whereas Scheme 2 has a 1 dB advantage over CC-QPSK-LFDMA. But with the compensation for power efficiency is taken into account, CC-QPSK-LFDMA scheme is the worst

performing of the three schemes, as Scheme 1 and Scheme 2 outperform it by 3.5 dB and 3.8 dB, respectively, at a BER of 10^{-5}.

The BER performances of the SC-FDMA schemes in the EVA and the ETU channel are shown in Fig. 6.5 and Fig. 6.6 respectively.
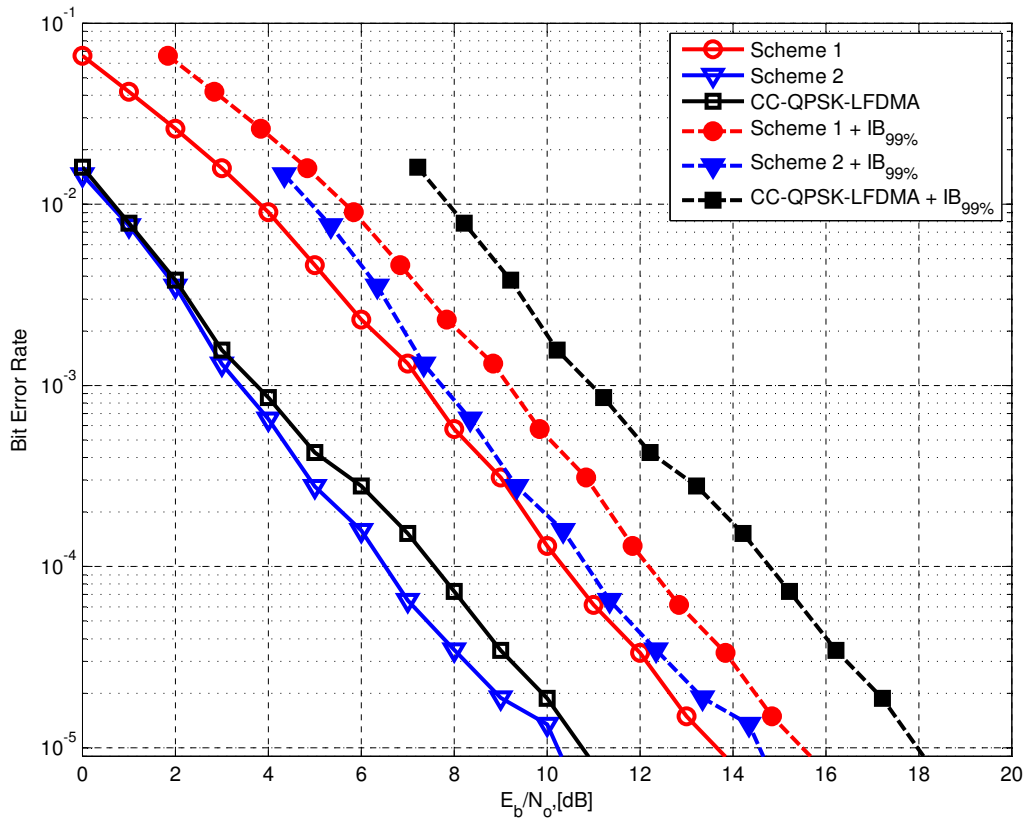

Figure 6.5. BER plots of CPM-SC-IFDMA Scheme 1, Scheme 2 and CC-QPSK-LFDMA in the EVA channel, assuming $J = 2$ users, $K = 150$ subcarriers per user and total subcarriers, $N_{\text{total}} = 300$ subcarriers. Open markers show the BER performance vs E_b/N_0. The filled-in markers show the BER performance vs $E_b/N_0 + \text{IB}_{99\%}$ using the $\text{IB}_{99\%}$ values from Table 6.1.
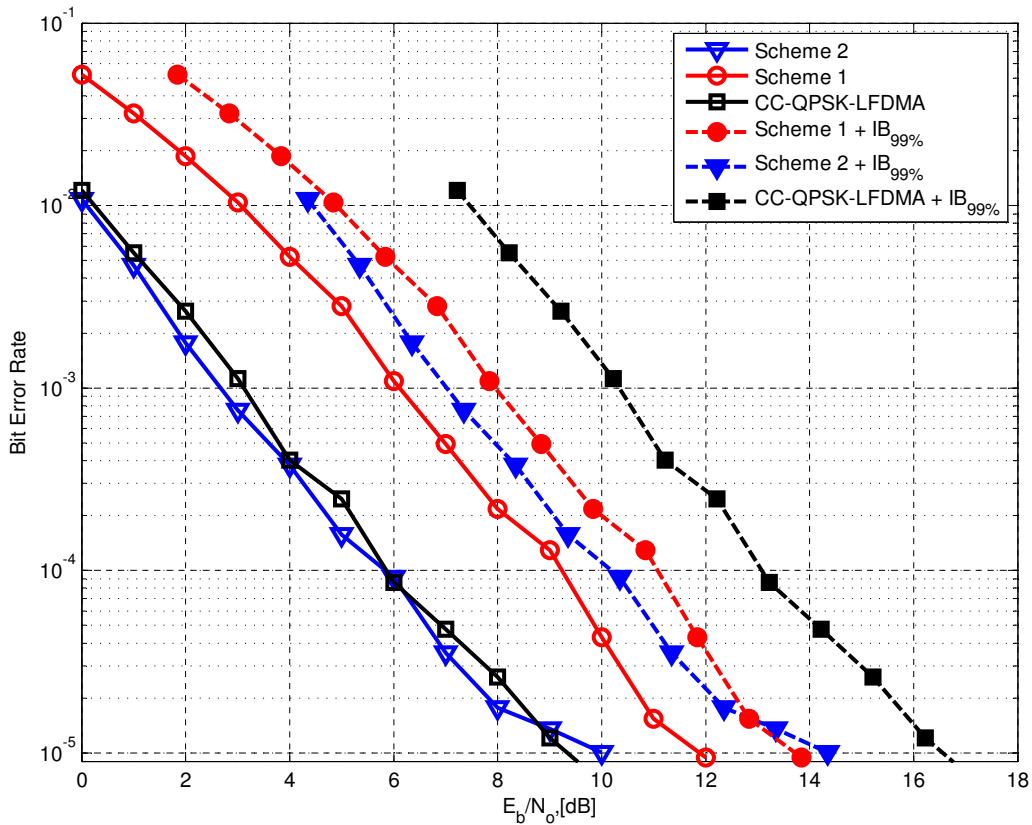
Figure 6.6. BER plots of CPM-SC-IFDMA Scheme 1, Scheme 2 and CC-QPSK-LFDMA in the ETU channel, assuming $J = 2$ users, $K = 150$ subcarriers per user and total subcarriers, $N_{\text{total}} = 300$ subcarriers. Open markers show the BER performance vs E_b/N_0. The filled-in markers show the BER performance vs $E_b/N_0 + \text{IB}_{99\%}$ using the $\text{IB}_{99\%}$ values from Table 6.1.

As we can see in these figures, in both channels, the CPM-SC-IFDMA schemes have a much better BER performance than the CC-QPSK-LFDMA scheme when the $\text{IB}_{99\%}$ values from Table 6.1 are added. In the ETU channel, at a BER of 10^{-5}, Scheme 1 has a 2.9 dB and Scheme 2 has a 2.3 dB advantage over the CC-QPSK-LFDMA scheme, and in the EVA channel Scheme 1 and Scheme 2 outperform the CC-QPSK-IFDMA scheme by 2.4 dB and 3.4 dB respectively.

Observing the BER plots of the SC-FDMA schemes in the AWGN and the three frequency selective channels, we see that when only raw BER values are

considered, CC-QPSK-LFDMA has almost similar performance as Scheme 2 and outperform Scheme 1 by a few dBs. Note that, it was pointed out in [4] and also shown in Section 6.2, that Scheme 1 has a much better spectral containment than both CC-QPSK-LFDMA and Scheme 2. After compensating for the power efficiency loss (adding in the $IB_{99\%}$ values from Table 6.1), the CC-QPSK-LFDMA scheme becomes the worst performing of all three SC-FDMA schemes.

Chapter 7

Conclusion and Future Work

In this work we have proposed CPM-SC-IFDMA, a new, power efficient transmission scheme that is suitable for uplink LTE. We have shown that when power efficiency is considered, the proposed scheme is more desirable than the current modulation-multiple access scheme specified for LTE. We have analyzed the PAPR simulation results and showed a comparison between the BER performance of CPM-SC-IFDMA and CC-QPSK-LFDMA, the scheme currently specified for LTE. The PAPR results show that the power efficiency advantage for the CPM-SC-IFDMA scheme can be as high as 7 dB (at 90% PAPR). Furthermore, the BER simulations indicate that CPM-SC-IFDMA outperform the CC-QPSK-LFDMA scheme by up to 3.8 dB (at a BER of 10^{-5}) when the power efficiency loss is taken into account (i.e., after adding the $IB_{99\%}$ values).

CPM-SC-IFDMA, therefore, is an attractive choice for uplink LTE, where reducing power consumption is the primary concern, in order to improve coverage and maximize the battery life of the mobile device. Also, as mentioned in [4], the CPM-SC-IFDMA scheme can be designed to demonstrate robust error performance by varying the different CPM parameters.

As we have discussed in Section 6.1, no studies have been conducted to find the numerically optimal CPM-SC-IFDMA scheme. Future work on CPM-SC-IFDMA would be to design an algorithm for finding the numerically optimal scheme. The performance of the CPM-SC-IFDMA scheme that we have demonstrated here, can be further improved with the numerically optimal scheme. Another interesting scope for future work can be the application of MIMO (Multiple Input and Multiple Output). Since LTE uses multiple antennas on both transmitter and receiver sides, analyzing the effect of MIMO on the simulation results can be a scope for future work.

Sponsor Acknowledgment

Appendix A

Derivation of time domain symbols of IFDMA and LFDMA

In this appendix we use the symbol notations described in Section 3.5. u_r ($r = 0, 1, \ldots, K-1$) represents the input symbols, U_k ($k = 0, 1, \ldots, K-1$) represents the outputs of the DFT operation, and v_l represents the output of the IDFT operation.

A.1 IFDMA

The subcarrier mapping process for IFDMA can be expressed as

$$
Y_q = \begin{cases} U_k, & q = kJ + i \\ 0, & otherwise \end{cases} \tag{A.1}
$$

where $i = 0, 1, \ldots, J-1$ is the user index. Let, $l = Kp + r$, for $0 \le r \le K-1$ and $0 \le p \le J-1$.

For the 0th user; i.e., for $i = 0$

$$v_l = v_{Kp+r}$$

$$= \frac{1}{N_{\text{total}}} \sum_{q=0}^{N_{\text{total}}-1} U_k e^{j2\pi \frac{lq}{N_{\text{total}}}}$$

$$= \frac{1}{N_{\text{total}}} \sum_{k=0}^{K-1} U_k e^{j2\pi \frac{lkJ}{N_{\text{total}}}}$$

$$= \frac{1}{KJ} \sum_{k=0}^{K-1} U_k e^{j2\pi \frac{lkJ}{KJ}}$$

$$= \frac{1}{J} \left[\frac{1}{K} \sum_{k=0}^{K-1} U_k e^{j2\pi \frac{Kp+r}{K}k} \right]$$

$$= \frac{1}{J} \left[\frac{1}{K} \sum_{k=0}^{K-1} U_k e^{j2\pi \frac{Kp}{K}k} e^{j2\pi \frac{r}{K}k} \right]$$

$$= \frac{1}{J} \left[\frac{1}{K} \sum_{k=0}^{K-1} U_k e^{j2\pi \frac{rk}{K}} \right] e^{j2\pi pk}$$

$$= \frac{1}{J} u_r$$

$$= \frac{1}{J} u_{(l)\text{mod K}} \tag{A.2}$$

For $i \neq 0$

$$v_l = \frac{1}{J} u_{(l)\text{mod K}} \cdot e^{j2\pi \frac{il}{N_{\text{total}}}} \tag{A.3}$$

A.2 LFDMA

The subcarrier mapping process for LFDMA can be expressed as

$$Y_q = \begin{cases} U_k, & 0 \leq k \leq K - 1 \\ 0, & K \leq k \leq N_{\text{total}} - 1 \end{cases} \tag{A.4}$$

Let, $l = Jr + p$, where $0 \leq r \leq K - 1$ and $0 \leq p \leq J - 1$. Then

$$v_l = v_{Jr+p}$$

$$= \frac{1}{N_{\text{total}}} \sum_{q=0}^{N_{\text{total}}-1} U_k e^{j2\pi \frac{lq}{N_{\text{total}}}}$$

$$= \frac{1}{N_{\text{total}}} \sum_{k=0}^{K-1} U_k e^{j2\pi \frac{lk}{N_{\text{total}}}}$$

$$= \frac{1}{JK} \sum_{k=0}^{K-1} U_k e^{j2\pi \frac{(Jr+p)k}{JK}} \tag{A.5}$$

If $p = 0$, then

$$v_l = v_{Jr}$$

$$= \frac{1}{JK} \sum_{k=0}^{K-1} U_k e^{j2\pi \frac{rk}{K}}$$

$$= \frac{1}{J} \left[\frac{1}{K} \sum_{k=0}^{K-1} U_k e^{j2\pi \frac{rk}{K}} \right]$$

$$= \frac{1}{J} u_r$$

$$= \frac{1}{J} u_{(l)\mathrm{mod\ K}} \tag{A.6}$$

If $p \neq 0$, since $U_k = \sum_{s=0}^{K-1} u_s e^{-j2\pi \frac{s}{K}k}$, then replacing U_k in (A.5) we can write

$$
\begin{aligned}
v_l &= v_{Jr+p} \\
&= \frac{1}{JK} \sum_{k=0}^{K-1} \left(\sum_{s=0}^{K-1} u_s e^{-j2\pi \frac{s}{K}k} \right) e^{j2\pi \frac{(Jr+p)k}{JK}} \\
&= \frac{1}{JK} \sum_{k=0}^{K-1} \left(\sum_{s=0}^{K-1} u_s e^{j2\pi \frac{Jr+p-sJ}{JK}k} \right) \\
&= \frac{1}{JK} \sum_{k=0}^{K-1} \left(\sum_{s=0}^{K-1} u_s e^{j2\pi \left\{ \frac{r-s}{K} + \frac{p}{JK} \right\}k} \right) \\
&= \frac{1}{JK} \sum_{s=0}^{K-1} u_s \left(\sum_{k=0}^{K-1} e^{j2\pi \left\{ \frac{r-s}{K} + \frac{p}{JK} \right\}k} \right) \\
&= \frac{1}{JK} \sum_{s=0}^{K-1} u_s \frac{1 - e^{j2\pi(r-s)}e^{j2\pi \frac{p}{J}}}{1 - e^{j2\pi \left\{ \frac{r-s}{K} + \frac{p}{JK} \right\}}} \\
&= \frac{1}{J} \left(1 - e^{j2\pi \frac{p}{J}} \right) \frac{1}{K} \sum_{s=0}^{K-1} \frac{u_s}{1 - e^{j2\pi \left\{ \frac{r-s}{K} + \frac{p}{JK} \right\}}}
\end{aligned}
\tag{A.7}
$$

So the time domain representation of LFDMA can be expressed as

$$
v_l = v_{Jr+p} = \begin{cases} \frac{1}{J} u_{(l)\mathrm{mod}\ K}, & p = 0 \\[3mm] \frac{1}{J} \left(1 - e^{j2\pi \frac{p}{J}} \right) \frac{1}{K} \sum_{s=0}^{K-1} \frac{u_s}{1 - e^{j2\pi \left\{ \frac{r-s}{K} + \frac{p}{JK} \right\}}}, & p \neq 0 \end{cases}
\tag{A.8}
$$

References

[1] J. G. Andrews, A. Ghosh, and R. Muhamed, *Fundamentals of WiMAX: Understanding Broadband Wireless Networking.* Prentice Hall Communication Engineering and Emerging Technologies Series, 2007.

[2] J. G. Proakis and M. Salehi, *Digital Communications.* McGraw-Hill, 2008.

[3] H. G. Myung and D. J. Goodman, *Single Carrier FDMA: A New Air Interface for Long Term Evolution.* Wiley series on wireless communication and mobile computing, 2008.

[4] M. Green, E. Perrins, and T. Svensson, "Introduction to CPM-SC-FDMA, a novel multiple-acess power-efficient transmission scheme," in *International Waveform Diversity and Design Conference, (Orlando, FL)*, Feb. 2009.

[5] *3rd Generation Partnership Project, 3GPP TS 25.101-Technical Specification Group Radio Access Network; User Equipment (UE) Radio Transmission and Reception (FDD)(Release 7)*, 2007.

[6] *3rd Generation Partnership Project, 3GPP TS 36.101-Technical Specification Group Radio Access Network; Evolved Universal Terrestrial Radio Access (E-UTRA); User Equipment (UE) Radio Transmission and Reception,(Release 8)*, 2008.

[7] M. Ergen, *Mobile Broadband; Including Wimax and LTE*. Springer, February 2009.

[8] H. Chen and M. Guizani, *Next Generation Wireless Systems and Networks*. John Wiley and Sons, Ltd, July 2006.

[9] H. Holma and A. Toskala, *LTE for UMTS; OFDMA and SC-FDMA Based Radio Access*. John Wiley and Sons, Ltd, 2009.

[10] *3rd Generation Partnership Project, 3GPP TR 25.913-Technical Specification Group Radio Access Network; Requirements for Evolved UTRA (E-UTRA) and Evolved UTRAN (E-UTRAN)(Release 9)*, 2009.

[11] *3rd Generation Partnership Project, 3GPP TS 36.101-Technical Specification Group Radio Access Network; Evolved Universal Terrestrial Radio Access (E-UTRA); Multiplexing and channel coding,(Release 9)*, 2008.

[12] *3rd Generation Partnership Project, 3GPP TS 36.101-Technical Specification Group Radio Access Network; Evolved Universal Terrestrial Radio Access (E-UTRA); Physical Channels and Modulation,(Release 9)*, 2008.

[13] H. G. Myung, J. Lim, and D. J. Goodman, "Peak-to-average power ratio of single carrier FDMA signals with pulse shaping," in *PIMRC'06*, 2006.

[14] H. G. Myung, "Single carrier fdma for uplink wireless transmission," *IEEE Vehicular Technology Magazine*, September 2006.

[15] J. B. Anderson, T. Aulin, and C. Sundberg, *Digital Phase Modulation*. New York, USA: Plenum Press, 1986.

[16] C. Sundberg, "Continuous Phase Modulation; a class of jointly power and bandwidth efficient digital modulation schemes with constant amplitude," *IEEE Communications Magazine*, vol. 24, April 1986.

[17] T. Aulin and C. Sundberg, "Continuous Phase Modulation-Part I: Full Response Signaling," *IEEE Transactions on Communication*, March 1981.

[18] ——, "Continuous Phase Modulation-Part II: Partial Response Signaling," *IEEE Transactions on Communication*, March 1981.

[19] E. Perrins and M. Cook, "A VHDL-Ready Telemetry Waveform Generator," Department of Electrical Engineering and Computer Science, University of Kansas, KS, Tech. Rep. 04-A, rev.03, September 2007.